Received: 25 August 2021 | Revised: 7 June 2022 | Accepted: 14 June 2022

DOI: 10.1002/glia.24231

GLIA

WILEY

RESEARCH ARTICLE

Repurposing the cardiac glycoside digoxin to stimulate myelin regeneration in chemically-induced and immune-mediated mouse models of multiple sclerosis

Haley E. Titus[1] | Huan Xu[2] | Andrew P. Robinson[1] | Priyam A. Patel[3] | Yanan Chen[2] | Damiano Fantini[4] | Valerie Eaton[1] | Molly Karl[5] | Eric D. Garrison[5] | Indigo V. L. Rose[6] | Ming Yi Chiang[1] | Joseph R. Podojil[1,7] | Roumen Balabanov[2] | Shane A. Liddelow[6] | Robert H. Miller[5] | Brian Popko[2] | Stephen D. Miller[1]

[1]Department of Microbiology-Immunology and the Interdepartmental Immunobiology Center, Northwestern University Feinberg School of Medicine, Chicago, Illinois, USA

[2]Neurology, Northwestern University Feinberg School of Medicine, Chicago, Illinois, USA

[3]Quantitative Data Science Core Center for Genetic Medicine, Northwestern University Feinberg School of Medicine, Chicago, Illinois, USA

[4]Urology, Northwestern University Feinberg School of Medicine, Chicago, Illinois, USA

[5]Department of Anatomy and Cell Biology, The George Washington University School of Medicine and Health Sciences, Washington, District of Columbia, USA

[6]Neuroscience Institute and Departments of Neuroscience, & Physiology, and Ophthalmology, New York University Grossman School of Medicine, New York, New York, USA

[7]Cour Pharmaceutical Development Company, Northbrook, Illinois, USA

Correspondence
Stephen D. Miller, Department of Microbiology-Immunology and the Interdepartmental Immunobiology Center, Northwestern University Feinberg School of Medicine, 303 E. Chicago Avenue, Chicago, IL 60611, USA.
Email: s-d-miller@northwestern.edu

Funding information
National Multiple Sclerosis Society, Grant/Award Numbers: FG20125-A-1(HET), RG1807-32005(BP); National Institutes of Health, Grant/Award Numbers: R21AI142059 (SDM), R01NS099334(SDM,BP), R01NS109372(BP)

Abstract

Multiple sclerosis (MS) is a central nervous system (CNS) autoimmune disease characterized by inflammation, demyelination, and neurodegeneration. The ideal MS therapy would both specifically inhibit the underlying autoimmune response and promote repair/regeneration of myelin as well as maintenance of axonal integrity. Currently approved MS therapies consist of non-specific immunosuppressive molecules/antibodies which block activation or CNS homing of autoreactive T cells, but there are no approved therapies for stimulation of remyelination nor maintenance of axonal integrity. In an effort to repurpose an FDA-approved medication for myelin repair, we chose to examine the effectiveness of digoxin, a cardiac glycoside (Na^+/K^+ ATPase inhibitor), originally identified as pro-myelinating in an in vitro screen. We found that digoxin regulated multiple genes in oligodendrocyte progenitor cells (OPCs) essential for oligodendrocyte (OL) differentiation in vitro, promoted OL differentiation both in vitro and in vivo in female naïve C57BL/6J (B6) mice, and stimulated recovery of myelinated axons in B6 mice following demyelination in the corpus callosum induced by cuprizone and spinal cord demyelination induced by lysophosphatidylcholine

(LPC), respectively. More relevant to treatment of MS, we show that digoxin treatment of mice with established MOG_{35-55}-induced Th1/Th17-mediated chronic EAE combined with tolerance induced by the i.v. infusion of biodegradable poly(lactide-co-glycolide) nanoparticles coupled with MOG_{35-55} (PLG-MOG_{35-55}) completely ameliorated clinical disease symptoms and stimulated recovery of OL lineage cell numbers. These findings provide critical pre-clinical evidence supporting future clinical trials of myelin-specific tolerance with myelin repair/regeneration drugs, such as digoxin, in MS patients.

KEYWORDS
digoxin, immune tolerance, multiple sclerosis, myelin regeneration, oligodendrocyte

1 | INTRODUCTION

Multiple sclerosis (MS) is the most common chronic inflammatory disease of the central nervous system (CNS) among young adults. Inflammatory demyelination and neurodegeneration lead to MS pathology; involving CNS infiltration of autoreactive T and B cells as well as influx/activation of inflammatory monocytes, macrophages, and microglia that attack myelin, oligodendrocytes (OLs), and axons (McFarland & Martin, 2007; Titus et al., 2020)

Effective long-term treatment of MS will require targeting three disease-associated drivers. First, self-tolerance must be re-established to specifically inhibit the underlying autoimmune pathology (Luo et al., 2016; McCarthy et al., 2014; Pearson et al., 2017; Pearson et al., 2019). Second, OLs and neurons within the CNS must be protected from degeneration. Third, myelin regeneration must be activated by stimulating oligodendrocyte precursor cells (OPCs) to differentiate/mature to remyelinate CNS axons (Rodgers et al., 2013).

While both the innate and adaptive immune systems are involved in MS pathogenesis (Weiner, 2009), $CD4^+$ T cells appear to primarily orchestrate the attack against the CNS. Naïve $CD4^+$ T cells are activated by professional antigen-presenting cells (APCs). APC-derived inflammatory cytokines induce differentiation of $CD4^+$ Th17 and Th1 cells, which produce cytokines that amplify the inflammation (Glass et al., 2010; Prinz & Kalinke, 2010). Currently available MS disease-modifying therapies are global immunomodulatory/immunosuppressants acting through non-specific inhibition of cell activation/function and/or trafficking. These drugs often have limited efficiency and are frequently associated with serious side effects. We have previously demonstrated that tolerance induced by the i.v. infusion of myelin antigen (Ag)-coupled or encapsulating PLG nanoparticles (PLG-Ag) effectively prevents and treats both chronic and relapsing–remitting experimental autoimmune encephalomyelitis (EAE) mouse models of MS by blocking activation and effector functions of pro-inflammatory effector Th1/17 cells (Getts et al., 2012; Getts et al., 2013; Hunter et al., 2014; McCarthy et al., 2017). Following our previous demonstration of successful tolerance induction using autologous myelin peptide-coupled autologous leukocytes in MS patients (Lutterotti et al., 2013), we have recently established safety and efficacy of PLG nanoparticles encapsulating gliadin for inducing tolerance in human celiac disease in a phase 1/2a clinical trial (Kelly et al., 2021).

The adult CNS exhibits a robust capacity for remyelination that has been demonstrated in both new inflammatory lesions and in older MS lesions with diminished inflammatory activity (Sim et al., 2002) yet normal myelin morphology (i.e., thickness) and function do not fully recover. Currently, there are no FDA-approved remyelination enhancing therapies for treatment of MS. A recent approach to accelerating identification of myelin regeneration drugs has been to screen existing FDA-approved small molecules in the NIH Clinical Collection in in vitro rodent myelination assays (Deshmukh et al., 2013; Lariosa-Willingham et al., 2016; Mei et al., 2014; Najm et al., 2015). Digoxin, a cardiac glycoside, used clinically to treat heart failure and arrhythmias, was identified as a potent myelin-promoting agent (Lariosa-Willingham et al., 2016). The cardiotonic steroids, Digoxin and Ouabain, are specific inhibitors of Na^+/K^+ ATPase (Laursen et al., 2015). Ouabain treatment of rats with CNS demyelination was previously shown to reverse slowed action potential velocities and to increase sensory evoked potentials (Kaji et al., 1988; Kaji & Sumner, 1989). Importantly, Ouabain improved evoked potential conduction velocities in MS patients with temperature sensitive symptoms (Kaji et al., 1990). A connection between the function Na^+/K^+ ATPase and changes in cell bioenergetics (i.e., aerobic glycolysis) has been demonstrated as well, indicating possible cell protective effects (Parker & Hoffman, 1967). As oligodendrocyte lineage cells shift bioenergetic processes (i.e., levels of aerobic glycolysis and oxidative phosphorylation) throughout differentiation as well as healthy versus stressed conditions (Agathocleous et al., 2012; Rao et al., 2017; Rone et al., 2016; Yanes et al., 2010), we thus chose to test the myelination stimulating capacity of digoxin in vitro and in vivo.

We demonstrate the capacity of digoxin to induce OPC differentiation in vitro, to robustly stimulate myelination in vivo in the chemically-induced cuprizone and lysophosphatidylcholine (LPC) demyelination/remyelination models, and in combination with PLG-Ag tolerance to ameliorate disease progression and promote recovery of OL lineage cell numbers in the immune-mediated MOG peptide-induced chronic experimental autoimmune encephalomyelitis (C-EAE) model.

2 | MATERIALS AND METHODS

2.1 | Experimental animals

Male & female neonatal C57BL/6J pups (Jackson Laboratories, Bar Harbor, ME) were used for primary OPC cultures and female adult mice were used for the various in vivo demyelinating disease models (cuprizone, LPC, and C-EAE). Male and female postnatal day 5 (P5) Sprague Dawley rat pups (Charles River) were used for astrocyte cell cultures. All procedures were performed with the approval of the Northwestern University, George Washington University, and New York University Institutional Animal Care and Use Committees and adhered to the NIH Guide for the Care and Use of Laboratory Animals.

2.2 | Primary mouse OPC isolation and culture

OPCs were isolated and cultured from C57BL/6J mice according to previously described immunopanning protocols with minor modifications (Emery & Dugas, 2013). Briefly, brains were extracted from male and female postnatal day 6 (P6) C57BL/6J mouse pups and dissociated in 200 U buffered papain (Worthington Biochemical, Lakewood, NJ) for 60 min at 37°C in 95% O_2, 5% CO_2, shaking gently every 15 min. Then papain buffer was removed, quenched in low then high ovomucoid solutions, and filtered to yield single cell suspensions. OPCs were purified by sequential immunopanning with anti-RAN2 to remove astrocytes, followed by anti-O1/GC to remove mature OLs, followed by positive selection plate anti-O4 for 45 min to yield OPCs. Cells were washed with EBSS, lifted with 0.025% trypsin for 3–4 min, washed, and 10^6 cells added to 10 cm^2 poly-D-lysine (Sigma-Aldrich, St. Louis, MO) coated plates in OPC growth medium with PDGF-α as previously described. Cultures were passaged three times prior to treatment. Neutral cultures, without PDGF-α, were treated with vehicle or digoxin (0.1, 1.0, or 10 ng/ml) for 48 hours (h) or 96 h. For OL differentiation, cultures were changed to differentiation medium, including T3 hormone, without PDGF-α. All groups (proliferation, neutral, neutral +0.1, 1.0, or 10 ng/ml digoxin, differentiation) had the same 3 biological samples ($n = 3$ pups pooled per biological sample) with technical replicates. Cells were collected on day 2 (d2) and day 4 (d4) for analysis.

2.3 | Immunocytochemistry of OL lineage cells

Conducted as previously described in (Xu et al., 2020). Briefly, the cells cultured on coverslips were rinsed with PBS and fixed with ice cold 4% PFA for 10 min at room temperature, washed with PBS, then air-dried and stored at −80°C until immunostaining. The primary antibody used was myelin basic protein Rabbit-anti-MBP (1:500, Abcam, Cat# ab40390) with secondary Donkey Anti-Rabbit IgG (H + L), Alexa Fluor 594 (Invitrogen, Cat # A-21207). DAPI stain in 405 was used for nuclear staining. Cells were imaged with a Mariana Yokogawa-type spinning disk confocal microscope using slidebook 6.0 (×64) software. All samples were imaged with the same parameters, followed by analysis of 20× images with ImageJ.

2.4 | OL mRNA analysis using microfluidics qPCR

Total RNA was isolated from mouse OL lineage cells (after digoxin treatment following the 2nd passage) using Aurum Total RNA Kit (Bio-Rad #732-6820) and measured by Nanodrop spectrophotometer. First, RNA quantity was determined with Qubit fluorometer. Total RNA examples were also checked for fragment sizing using Agilent Bioanalyzer 2100. RNA integrity was verified using Agilent chip (Agilent Technologies). cDNA was generated using iScript cDNA Synthesis Kit (Bio-Rad #1708890) following the manufacturer's protocol. Real-time polymerase chain reaction (PCR) was performed on the cDNA using iQ SYBR Green Supermix (Bio-Rad #1708882) using a Quantstudio 7 (Thermo fisher) 384 well system. Each sample was analyzed in triplicate. Relative expression from amplified cDNA samples was determined using the $2^{-\Delta\Delta}{}_{CT}$ method (Pfaffl, 2001). The expression of the selected transcripts (e.g., *Pdgfr-α*, F:CGATGACTAAGGAATCGGTCA and R:CAACCACA CTCAGACGGATG) was normalized to the housekeeping gene glyceraldehyde-3-phosphate (*Gapdh*, F:TGTGTCCGTCGTGGATCTGA & R:TTGCTGTTGAAGTCGCAGGAG) cDNA.

2.5 | Astrocyte purification and culture

Astrocytes were purified by immunopanning from male and female P5 Sprague Dawley rats and cultured as previously described (Foo et al., 2011). Briefly, cortices were dissociated mechanically with scalpel, then enzymatically with papain to generate a single-cell suspension that was incubated on successive negative immunopanning plates to remove microglia, endothelial cells, and oligodendrocyte lineage cells before positively selecting for astrocytes with an ITGB5-coated panning plate. Cells were plated at 5000 cells/well and cultured in a defined, serum-free base medium containing 50% neurobasal, 50% DMEM, 100 U/ml penicillin, 100 μg/ml streptomycin, 1 mM sodium pyruvate, 292 μg/ml L-glutamine, 1× SATO and 5 μg/ml N-acetyl cysteine. This medium was supplemented with the astrocyte-required survival factor HBEGF (Peprotech, 100-47) at 5 ng/ml. After 1 week, astrocytes were treated with 0.1, 1.0, or 10.0 ng/ml digoxin. After 24 h (d1), 48 h (d2), or 96 h (d4) cells were imaged with a Incucyte (R) Zoom live imaging system then washed in 1× PBS, lysed, and total RNA collected using the RNeasy Mini Kit (Qiagen). All samples were imaged with the same parameters, followed by blinded analysis of 20× phase contrast images with ImageJ. For cell number, quantified four regions of interest (ROIs) per biological replicate ($n = 3$) in all treatment groups ($n = 4$). For cell processes, quantified 10 cells per ROI, with 4 ROIs per biological replicate ($n = 3$) in all treatment groups ($n = 4$),

2.6 | Astrocyte mRNA analysis using microfluidics qPCR

Total RNA was extracted from astrocyte cell cultures using β-mercaptoethanol and RLT Buffer (Qiagen) and a rubber policeman by normal supplier protocol for RNA extraction (RNEasy kit, Qiagen). RNA samples were prepared as previously described (Liddelow et al., 2017), cDNA conversion (qScript™ cDNA SuperMix, Quanta-Bio), pre-amplification for genes of interest (STA Mastermix, Applied Biosystems 44-885-93), removal of excess primers (Exonuclease I, New England BioLabs M0293L), and dilution of sample. Five microliters of sample mix containing pre-amplified cDNA and amplification Master mix (20 mM MgCl2, 10 mM dNTPs, FastStart Taq polymerase, DNA-binding dye loading reagent, 50× ROX, 20× Evagreen) was loaded into each sample inlet of a 96.96 Dynamic Array chip (Fluidigm Corporation), and 5 μl from an assay mix containing DNA-assay loading reagent, as well as forward and reverse primers (10 pmol/μl) was loaded into each detector inlet. Dynamic array chips were mixed and loaded using a Nano-FlexTM 4-IFC Controller (Fluidigm) before processing the chip in a BioMark HD Real-Time PCR System (Fluidigm) using the standard fast program. Data were collected using BioMark Data Collection Software 2.1.1 build 20090519.0926 (Fluidigm) as the cycle of quantification, where the fluorescence signal of amplified DNA intersected with background noise. Fluidigm data were corrected for differences in input RNA using the mean of the reference gene *Rplp0*. Data preprocessing and analysis was completed using Fluidigm Melting Curve Analysis Software 1.1.0 build 20100514.1234 (Fluidigm) and Real-time PCR Analysis Software 2.1.1 build 20090521.1135 (Fluidigm) to determine valid PCR reactions. Invalid reactions were removed from later analysis. All primer sequences have been published elsewhere (Liddelow et al., 2017).

2.7 | Digoxin treatment

(12β-hydroxydigitoxin, Sigma D6003) was used to make a stock of 1 mg/ml weekly in DMSO and stored at 4°C. Mice were injected intraperitoneal (i.p.) with 100 μl of 0.3 mg/kg (6 μg stock DMSO in 100 μl dH_20); based on literature in rat models (Kaji & Sumner, 1989) and validation in adult female C57BL/6J mice in vivo safety testing (initially as an outcome of no detrimental change in weight, further analysis throughout the manuscript). Vehicle used in all experiments is 6% DMSO (6 μl/100 μl of dH_20).

2.8 | Lysophosphatidylcholine-induced spinal cord focal demyelination/remyelination model

A 10-week-old female C57BL/6J mice ($n = 36$) were anesthetized with isoflurane and underwent a partial laminectomy to access the dorsal aspect of the thoracic spinal cord, at the level of T10-T12. Of which 18 sham control mice received 1 μl of 0.9% saline and 18 mice received 1 μl of 1% LPC (L4129, Sigma) into the dorsal white matter. Performed blinded, beginning 1 day post-LPC injection 9 mice in each group were treated with vehicle and 9 mice were treated with digoxin (0.3 mg/kg/qad IP) every other day through day 9 and sacrificed on day 10. Spinal cord tissue was examined in 3–6 per group as described (Keough et al., 2015; Robinson et al., 2020). Lesioned areas were sectioned and stained for myelin using Luxol fast blue or toluidine blue. Quantitation of myelinated axon counts was conducted on 63× images of lesion sections by manually counting the number of thinly-wrapped (2–4 wraps) axons within lesion boundaries in 500–800 axons/animal ($n = 4$–6 mice/genotype), in blinded fashion. Further myelination analysis was performed using FEI Helios focused ion beam scanning EM (FIBSEM) and images were acquired using Thermo Fisher Maps 3.11 software. Images were stitched at a magnification of 10,000×, with a dwell time of 5 μs and a resolution of 3072 × 2048 pixels encompassing the 2D lesion area. Immunohistochemistry (IHC) analysis was performed on the remaining three mice per group (Caprariello et al., 2015).

2.9 | Immunohistochemistry of spinal cord sections

Spinal cord tissue from 4% paraformaldehyde-perfused mice was post-fixed in PFA and then cryopreserved in 30% sucrose. Tissue was embedded in optimal cutting temperature (OCT) and sectioned to a thickness of 20 μm, using a Leica CM 1950 cryostat. Slides were stored at −80°C until staining. Cryostat sections were air dried processed for mature OLs (CC1, Calbiochem #OP80), myelin basic protein (MBP, Biolegend #SMI-99), and astrocytes (GFAP, DAKO #Z0334) markers. Fluorescent secondary antibodies (Invitrogen, Alexa Fluor H + L, species specific) used were alexa 564 (CC1, MBP, GFAP). DAPI stain in 405 was used for nuclear staining. Slides were mounted in Vectashield Mounting Media (Vector Labs #H-1000). Standard fluorescent images were captured with a Leica DM5500 B microscope using a Leica DFC 500 camera using a 20× objective with filters/lasers (405, 488, and 565 nm) and ImageJ software. Counting was performed blinded on three mice per group using an ImageJ micromanager plugin. Images collected for fluorescence intensity were taken on a Zeiss Cell Observer Spinning Disk Confocal microscope at 40×, with Photometrics Delta high-speed EM CCD cameras and Imaris software.

2.10 | Cuprizone-induced corpus callosum demyelination/remyelination model

A 8-week-old female C57BL/6J mice were fed either control chow or 0.2% cuprizone chow (Envigo Labs, Catalog #TD.01453) for 6 weeks. At the end of 6 weeks (age 14 weeks), all mice in both groups were fed control chow. The 36 mice in each group were then further divided into 18 mice each, to begin receiving either vehicle or digoxin (0.3 mg/kg qad i.p.) at d0. On days 7 (6 + 1 week), 14 (6 + 2 weeks), and 21 (6 + 3 weeks), 3 mice per group were perfused with 4%

paraformaldehyde and 2.5% glutaraldehyde and CNS tissue (corpus callosum) prepared for electron microscope (EM) imaging. Ultrathin sections were stained in uranyl acetate and lead citrate, then photographed on a FEI Spirit G2 TEM microscope using Tecnai imaging & analysis (TIA) software. We measured g-ratios of all myelinated fibers from electron micrographs, by dividing the diameter of each axon by the fiber diameter (diameter of the axon together with its myelin sheath) in 300–500 axons/animal ($n = 3$ mice/group), using ImageJ software. Quantification was carried out blinded. The remaining three mice per group at each assay time were perfused with PBS and forebrain tissue processed for flow cytometric analysis of glial cells (Praet et al., 2014).

2.11 | Tolerance induction with MOG_{35-55}-encapsulating PLG nanoparticles

PLG-MOG_{35-55} and PLG-$OVA_{323-339}$ nanoparticles were prepared by double-emulsion, solvent drying and characterized as previously described (Hunter et al., 2014; McCarthy et al., 2017; Smarr et al., 2016). The z-average size of the nanoparticles was 483.7 nm. The zeta potential was −84.7 ± 14.3 mV. Tolerance was induced by i.v. injection of 2.5 mg of nanoparticles encapsulating 15.685 μg MOG_{35-55} in 0.2 ml of D-PBS.

2.12 | Active and adoptive C-EAE

A 8-week-old C57BL/6J female mice were injected s.c. with 200 μg of MOG_{35-55} peptide or $OVA_{323-339}$ (as an antigen-specificity control) (Genemed Synthesis, San Francisco, CA) emulsified in complete Freund's adjuvant (CFA) containing 200 μg of *Mycobacterium tuberculosis* H37Ra (Difco, Detroit, MI) distributed over three sites on the flank. For transfer EAE, spleen and inguinal lymph nodes collected on day 8 post-MOG_{35-55} immunization were reactivated with 20 μg/ml of MOG_{35-55} and 10 ng/ml recombinant murine IL-12 (R&D Systems) for 72 h. Following culture, cells were collected, labeled with Cell Trace CFSE dye (Thermo Fisher), 3×10^6 cells were transferred to recipient mice. In both models, 200 μg pertussis toxin (List, Campbell, CA) was administered i.p. on day 0 (d0) and day 2 (d2). Clinical signs of EAE were assessed daily according to the following scores: 0, no clinical sign of disease; 1, limp tail; 2, hind limb weakness; 3, partial hind limb paralysis; 4, complete hind limb paralysis; 5, hind and fore limb paralysis. Data are reported as the mean daily clinical score ± *SEM* (Terry et al., 2016).

2.13 | Ex vivo T cell proliferation and cytokine analysis

At the indicated times, spleens were collected from 3 to 6 individual C57BL/6J mice per treatment group and the total splenocytes were cultured ex vivo in 96-well plates (10^6 cells per well) with either MOG_{35-55} or $OVA_{323-339}$ (10 μg/ml) or anti-CD3 (1 μg/ml) (McCarthy et al., 2017). Two identical sets of culture plates were prepared. One set was pulsed with 1 μCi of ^{3}H-TdR at 48 h and harvested at 72 h to determine cell proliferation. Supernatants were collected from the second set at 48 h and levels of peptide-specific cytokine production determined by Luminex LiquiChip (Millipore)

2.14 | Flow cytometry

CNS cell populations were quantitated by flow cytometry. OPCs from P5-7 C57BL/6J neonatal mouse pups were immunopanned, passaged twice, and treated with vehicle or digoxin (0.1, 1.0, or 10 ng/ml) for 48 or 96 h prior to analysis. Mouse brain tissue from PBS perfused mice was dissociated/processed to yield single cell suspensions for flow cytometry analysis following Percoll density gradient separation as previously described (Robinson et al., 2014). Cells were washed, resuspended in FACS buffer (PBS with 2% FCS) and counted. Fc receptors were blocked using anti-mouse CD16/32 (0.25 μg; eBioscience #14–0161-86). Cells were then immunostained for 60 min at 4°C using the following specified antibodies: early glial progenitors (A2B5 1:100; R&D Systems #MAB1416), late glial progenitors (PDGFRα 1:50; Millipore #CBL1366 & NG2 1:200; Millipore #AB5320), pre-OL to pre-myelinating OL (O4 1:100; Millipore #MAB345), pre-myelinating OL to myelinating OL (GalC 1:100; Millipore #MAB342), myelinating OL (MOG, 1:100; Millipore #MAB5680), astrocytes (GLAST- APC 1:10; Miltenyi Biotec #130-095-814), and blood/microglia (CD45 V500 1:100; BD Biosciences #561487). The above indicated purified antibodies for the oligodendrocyte lineage cells were conjugated to Atto 488, PE-Cy7, PerCP Cy 5.5, APC-Cy7, Atto700, and PE respectively, using Lightning-Link Antibody Labeling Kits (Novus Biologicals #350-, 762-, 763-, 765-, 354-, 703-0005). Live/dead cell stain (1:1000; Invitrogen L34955) and Annexin V 350 (1:20, Life technologies A23202) were used to exclude non-viable cells. Flow cytometry was performed on an LSR Fortessa using FacsDiva software for acquisition. Analysis was performed using FlowJo10 software (TreeStar). Compensation was completed using positive and negative controls as well as fluorescent minus one (FMO) samples. Enumeration of live CNS-resident was performed using the following markers: early OPCs ($A2B5^+$), late OPCs ($PDGFR\alpha^+$, $NG2^+$), pre-OLs to pre-myelinating OLs ($O4^+$), pre-myelinating OLs to myelinating OLs ($GalC^+$), and myelinating OLs (MOG^+). Cell populations, per sample ($n = 3$–6 mice/group) were quantified.

2.15 | Total RNA-sequencing

Total RNA was isolated from mouse OL lineage cells (after treatment following the 2nd passage) using Aurum Total RNA Kit (Bio-Rad #732-6820). Total RNA was isolated from snap-frozen mouse CNS tissue using homogenization and the RNeasy Lipid Tissue Mini Kit (Qiagen 74804). RNA concentration was measured by Nanodrop

spectrophotometer. The stranded total RNA-seq was conducted in the Northwestern University NUSeq Core Facility. First, RNA quantity was determined with Qubit fluorometer. Total RNA examples were also checked for fragment sizing using Agilent Bioanalyzer 2100. Illumina TruSeq Stranded Total RNA Library Preparation Kit was then used to prepare sequencing libraries without modification to the kit procedure. Briefly, this procedure includes rRNA depletion, cDNA synthesis, 3′ end adenylation, adapter ligation, library PCR amplification and validation. Lllumina NextSeq 500 Sequencer was used to generate single-end, 75 bp reads sequence from the libraries. The quality of DNA reads, in fastq format, was evaluated using FastQC (Andrews, 2010). Adapters were trimmed, and reads of poor quality or aligning to rRNA sequences were filtered using Trim Galore (http://www.bioinformatics.babraham.ac.uk/projects/trim_galore/). The cleaned reads were aligned to the mouse genome (mm10) using STAR (Dobin et al., 2013). Read counts for each gene were calculated using HTSeq-Counts (Anders et al., 2015) in conjunction with a gene annotation file for mm10 obtained from Ensembl (http://useast.ensembl.org/index.html). A comprehensive QC report was generated using MultiQC (Ewels et al., 2016) Differential expression was determined using DESeq2 (Love et al., 2014) The cutoff for determining significantly differentially expressed genes was an FDR-adjusted *p*-value less than .05. The pathway analysis was done using Metascape (Zhou et al., 2019) and the Venn diagrams were generated using InteractiVenn (Heberle et al., 2015). Data will be made publicly available through deposit on the NIH NCBI Gene Expression Omnibus (GEO).

2.16 | Statistical analysis

Data are presented as mean ± *SEM* unless otherwise noted. To compare flow cytometry data collected on multiple days, data were represented as fold change compared to the control. Prism 6 software (GraphPad) was used for all statistical analyses. Comparison between two groups (i.e., genotypes, treatments) was done via Student's *t* tests using a significance cutoff of $p < .05$ ($^{*}p \le .05$, $^{**}p \le .01$, $^{***}p \le .001$, $^{****}p \le .0001$). For comparison of three or more groups, one-way ANOVA or two-way ANOVA followed by Tukey post hoc tests were performed using a significance cutoff of $p < .05$ ($^{*}p \le .05$, $^{**}p \le .01$, $^{***}p \le .001$, $^{****}p \le .0001$). Complete statistical analysis is detailed in Table S1.

3 | RESULTS

3.1 | Effects of digoxin treatment on gene expression and differentiation of C57BL/6J OPCs in vitro

Recent data demonstrate the robust ability of several FDA-approved drugs, including digoxin, to promote OPC differentiation in vitro (Lariosa-Willingham et al., 2016; Mei et al., 2014; Najm et al., 2015). Digoxin was identified in a small molecule screen of mixed male and female rat OPCs co-cultured with retinal ganglion neurons as well as using a heterogeneous mixture of bulk embryonic rat cortex cells (Lariosa-Willingham et al., 2016). We first used RNA-seq to determine transcriptome changes in OL lineage cells treated with digoxin. Proliferating mixed male and female C57BL/6J mouse neonatal forebrain OPC cultures were changed to media without PDGF and treated with vehicle (termed Neutral), the indicated concentrations of digoxin (0.1, 1.0, or 10 ng/ml), or T3 (differentiation control) for 48 h (d2) or 96 h (d4). Cells were snap-frozen and total RNA was isolated

Principal component analysis (PCA) showed variation in gene signatures within and between groups (treatments and timepoints) (Figure 1a). Within group variance was low as the groups cluster tightly within treatments per timepoint. Proliferation groups clustered tightly from day 2 (d2) and day 4 (d4). Neutral and Differentiation cultures progressed toward differentiation and maturation of the OL lineage over time, and anticipated variance between d2 and d4 is noted for all groups. Neutral cultures showed differentiation over time and therefore had wide variance between the d2 and d4 (expected peak differentiation) groups. Of note, there was more variance between Neutral samples with digoxin treatment (10 ng/ml) when compared to vehicle at d2 (Figure 1a). Volcano plots showed all differentially expressed genes in Neutral (N) versus digoxin treatment (10 ng/ml) (ND10) and Neutral (N) versus Differentiation (T3) at d2 (Figure 1b, significant in red). The Venn diagram indicated the number of significant differentially expressed genes (up or down regulated) as compared to N, unique or shared by ND10 and T3 at d2 (Figure 1c). There was overlap of genes up regulated in both, down regulated in both, conversely regulated in both, or only significantly expressed within either group. The cumulative overlap of differentially expressed genes was visualized through a Circos Plot of the same genes shared (purple lines) and functional overlap of different genes that fall into the same ontology term (blue lines) (Figure 1d). The heatmap of enriched terms indicated the top 20 common pathways of the Neutral + digoxin (ND10) and differentiation (T3) groups at d2 (Figure 1e).

Highlighting the effect of digoxin on the OL cell lineage at d2, the heatmap showed relative expression (up or down regulation, orange or blue) of genes based on expected trends, including; early oligodendrocyte lineage genes (green) as well as oligodendrocyte differentiation and maturation genes (purple) (Figure 2a). Interestingly, there were significant differences in changes in expression of the OL lineage genes in (T3) and (ND10) conditions at d2 (Figure 2a). T3, the positive control for differentiation, led to a decrease in early OL lineage genes (green – *Nkx2-2*) as well as an increase in OL differentiation and maturation genes (purple – *Ermn*, *Ninj2*, *Gjb1*, *Cldn11*, *Mal*) compared to neutral; distinct from ND10. Of note, ND10 led to a decrease in early OL lineage genes (green - *St18*, *Spon1*, *Matn4*, *Rlbp1*, *Cdo1*, *Rnf180*) as well as an increase in OL differentiation and maturation genes (purple – *Cnp*, *Omg*, *Gpr62*, *Gal3st1*) compared to neutral; distinct from T3. These data indicated a significant down regulation of new OL and OPC genes as well as an up regulation of differentiation and maturation genes induced by treatment with 10 ng/ml digoxin.

The circos plot highlighted the strong overlap in genes differentially expressed in T3-induced differentiation conditions (T3) and genes induced by treatment with 10 ng/ml digoxin (ND10) (Figure 1d). In both

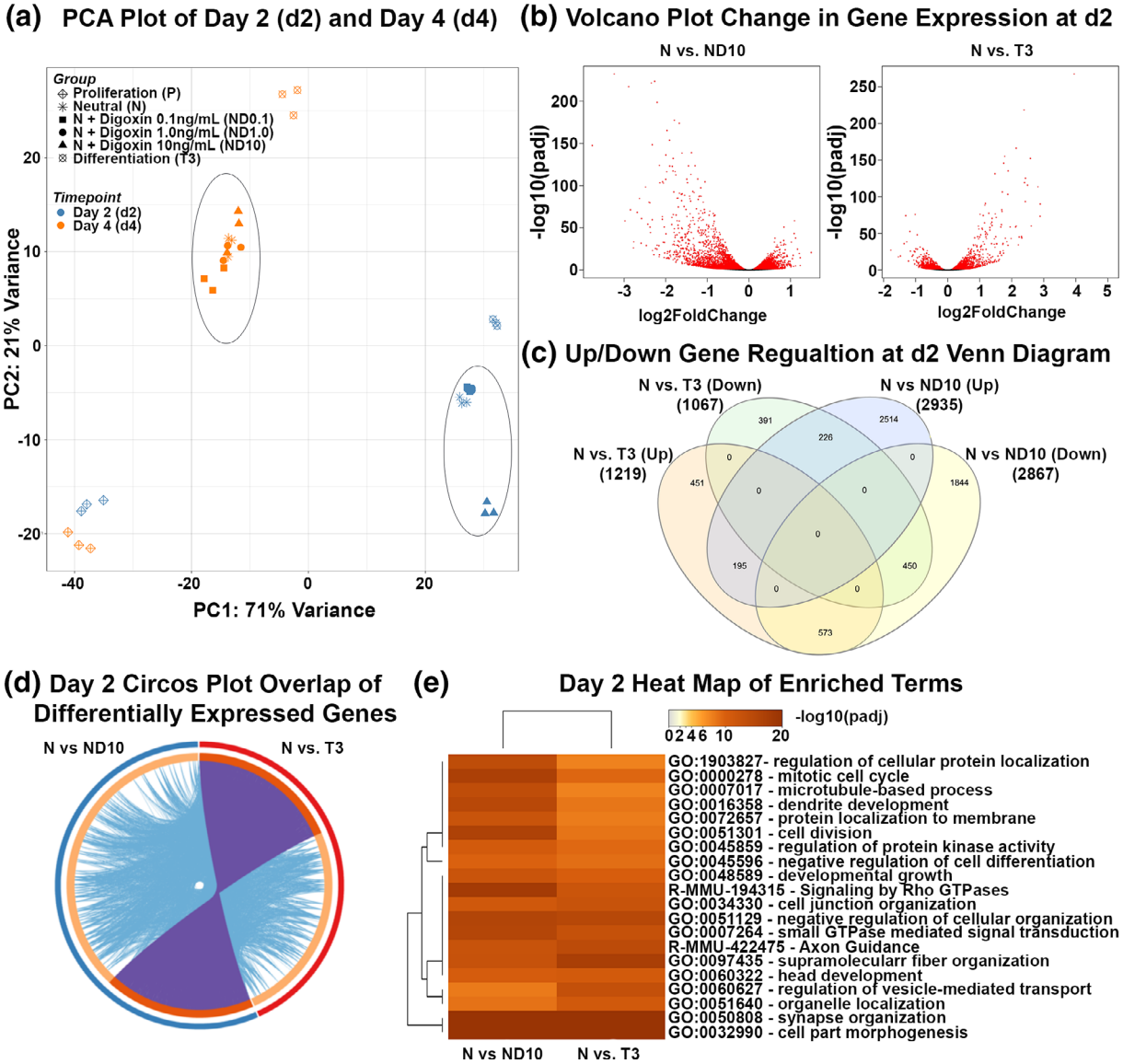

FIGURE 1 Effects of digoxin treatment on gene expression of C57BL/6J OPCs in vitro. Proliferating mixed male and female C57BL/6J mouse OPC cultures, including PDGF, were passaged two times prior to treatment. OPC cultures were changed to media without PDGF and treated with vehicle (termed neutral), the indicated concentrations of digoxin (0.1, 1.0, or 10 ng/ml), or T3 (differentiation control). Total RNA was isolated from snap-frozen OL lineage cells at 48 h (d2) or 96 h (d4). Principal component analysis (PCA) of variation of gene expression within and between treatment groups and time points. Horizontal and vertical axis show two principal components that explain the greatest proportion (71% and 21%) of variation (a). Volcano plots display the differentially expressed genes at d2. The y-axis corresponds to the FDR adjusted *p*-value ($-\log_{10}$) and the x-axis displays the fold change ($\log_2$). The red dots represent the significant genes. Positive x-values represent up-regulation and negative x-values represent down-regulation (b). Venn diagram displays the number of significantly differentially expressed genes (up or down regulated) at d2. Differential expression was determined using DESeq2 and the cutoff for determining significantly differentially expressed genes was an FDR-adjusted $p < .05$ (c). Circos plot shows the overlap between gene lists, where purple curves link identical genes and blue curves link genes that belong to the same enriched ontology term. The inner circle represents gene lists, where hits are arranged along the arc. Genes that hit multiple lists are colored in dark orange, and genes unique to a list are shown in light orange (d). Heatmap shows the top 20 enriched clusters across d2 colored by significance, FDR adjusted *p*-value (−log10) (e).

groups there was a decrease in expression of early OL lineage genes (green - *Olfm2*, *Slitrk1*, *Cspg4*, *Pdgfra*) as well as an increase in expression of OL differentiation and maturation genes (purple - *Shisa4*, *Mbp*, *Nkx6-2*) compared to neutral (Figure 2a). The significant decrease in *Pdgfra* at d2 in all groups compared to proliferation (****$p < .0001$) and ND10 compared to N (*$p = .0357$) was confirmed via qPCR (Table S1).

The significant increase in myelin basic protein levels induced by digoxin and T3 were confirmed by immunofluorescent staining of d4 coverslip cultures (Figure 2b,c). There was not a significant difference in the MBP MFI between ND10 and T3 at d4. Further analysis showed no significant difference in the total number of ($DAPI^+$) cells between N, ND10, T3 groups (Figure 2d, Table S1),

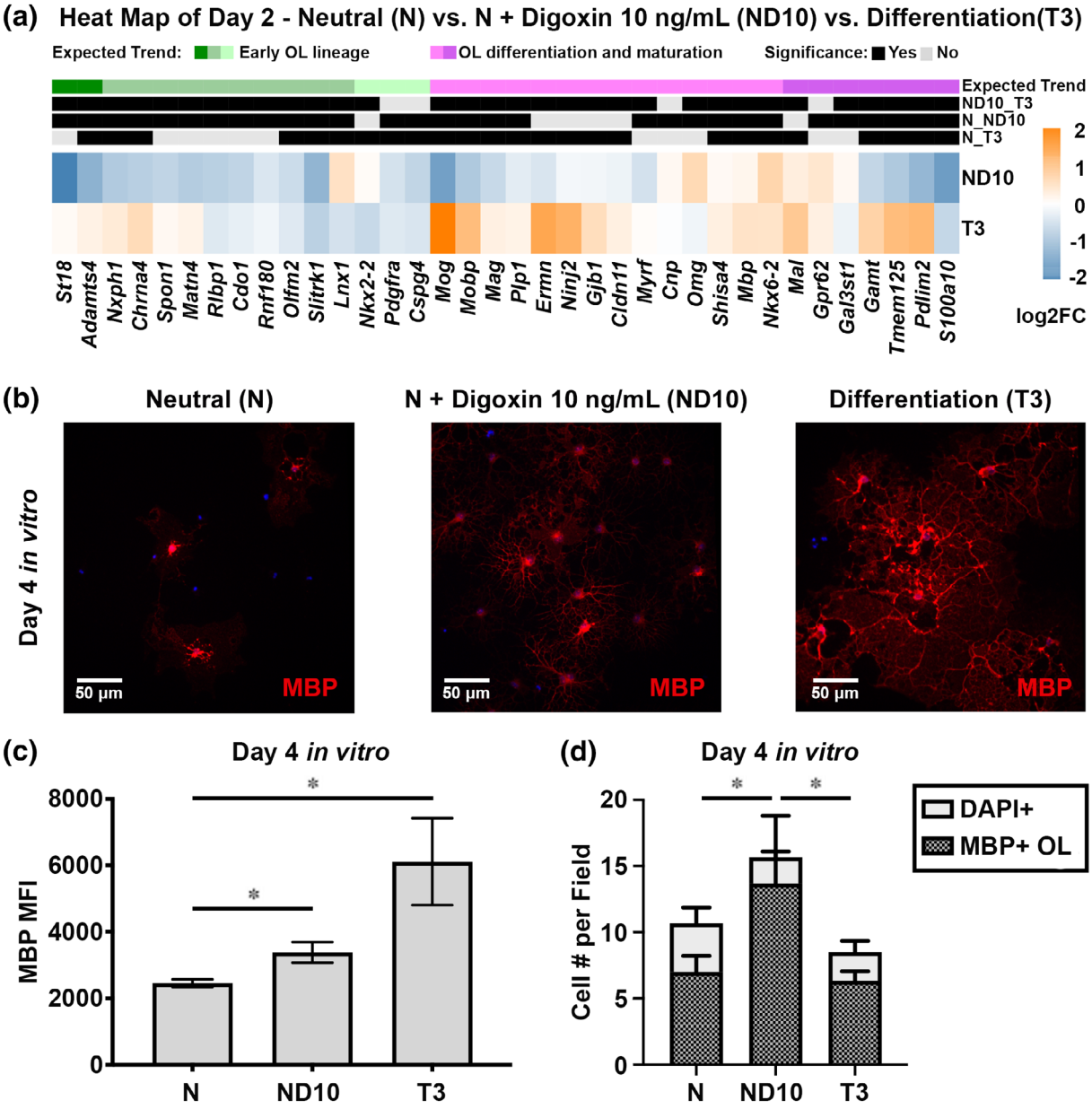

FIGURE 2 Effects of digoxin treatment on differentiation of C57BL/6J OPCs in vitro. Heatmap shows relative expression of genes as fold change (log_2) based on expected trend at d2. Orange color indicates relative upregulation, whereas blue indicated relative down regulation. Row annotations mark different expected trends, including early OL lineage genes (green) and OL differentiation and maturation genes (purple). Genes that were significantly differentially expressed are marked in black (a). Immunofluorescent staining of myelin basic protein (MBP) was carried out with representative images for the various treatment groups shown (b) and MBP staining quantitated with results presented as mean fluorescent intensity (MFI) (c) as well as cell number co-labeling with nuclear staining (DAPI) (d) ($n = 3$ biological samples/group with $n = 2$ technical replicates). (*$p < .05$).

however, there was a significant increase in the number of mature MBP^+ OLs in ND10 compared to N or T3 (Figure 2d, Table S1). This change in ND10 compared to N can also be noted as a significant increase in %MBP/DAPI (Table S1). Therefore, the increase in MBP MFI in ND10 is associated with an increase in MBP^+ OLs and % MBP/DAPI. T3 MBP^+ OLs and %MBP/DAPI are not significantly different compared to N, therefore highlighting there is more MBP per cell. In summary, digoxin promoted differentiation of OPCs in culture, as measured via downregulation of OPC genes and upregulation of OL genes at d2 (Figure 2a), resulting in an increase in differentiation and maturation at d4 compared to vehicle treated cells (Figure 2b–d).

3.2 | Effects of digoxin on myelin in naïve female C57BL/6J mice and regeneration in mice treated after cuprizone-induced demyelination

As digoxin promoted the differentiation and maturation of OL lineage cells in vitro, we asked if it could promote OL differentiation and

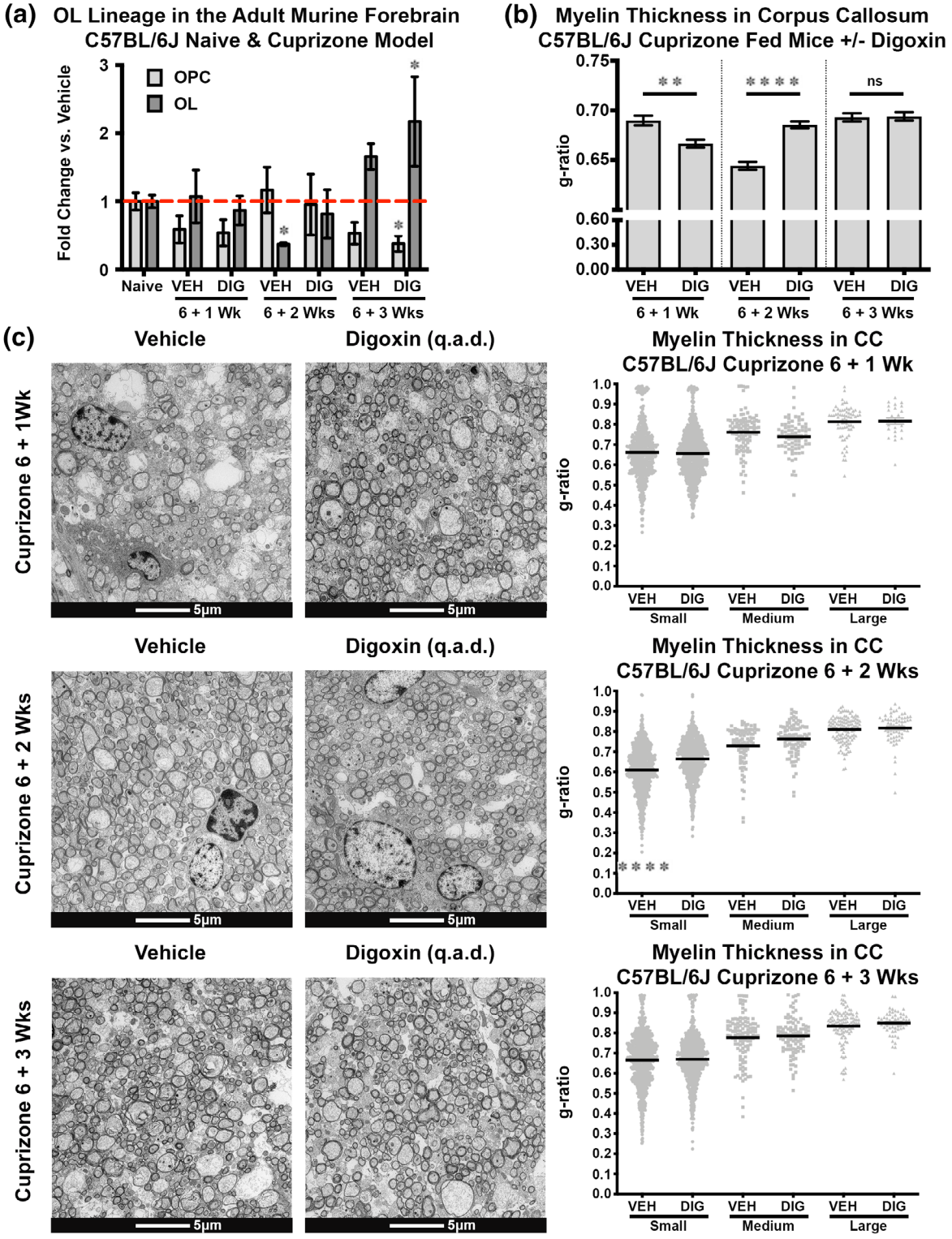

FIGURE 3 Digoxin treatment promoted earlier myelin regeneration in the brains of female C57BL/6J mice following cuprizone-induced demyelination. 8-week-old female C57BL/6J mice were fed control or cuprizone chow for 6 weeks and then placed on normal chow and treated i.p. with vehicle (VEH) or digoxin (DIG) 0.3 mg/kg qad. Flow cytometric analysis of mouse forebrain early OPCs ($A2B5^+$) and OLs ($GalC^+$) (measured as fold change vs. vehicle) after 1, 2, and 3 weeks of digoxin administration (a). Measurement of g-ratios of all myelin fiber sizes was performed blinded on midline sections of the corpus callosum after 1, 2, and 3 weeks of digoxin treatment ($n = 300–500$ axons per mouse, $n = 3$ mice/group) (b). Measurement of g-ratios of small (0.1–0.89 μm), medium (0.9–1.19 μm), and large (>1.2 μm) myelin fibers in midline sections of the corpus callosum after 1, 2, and 3 weeks of digoxin treatment ($n = 300–500$ axons per mouse, $n = 3$ mice/group). Representative electron micrograph per experimental group (1900×) within the vehicle (left) versus digoxin treatment (right) groups (c). (*$p < .05$, **$p < .01$, ***$p < .001$, ****$p < .0001$, ns, not significant). Extended data for Figure 3 is labeled as Figure S1.

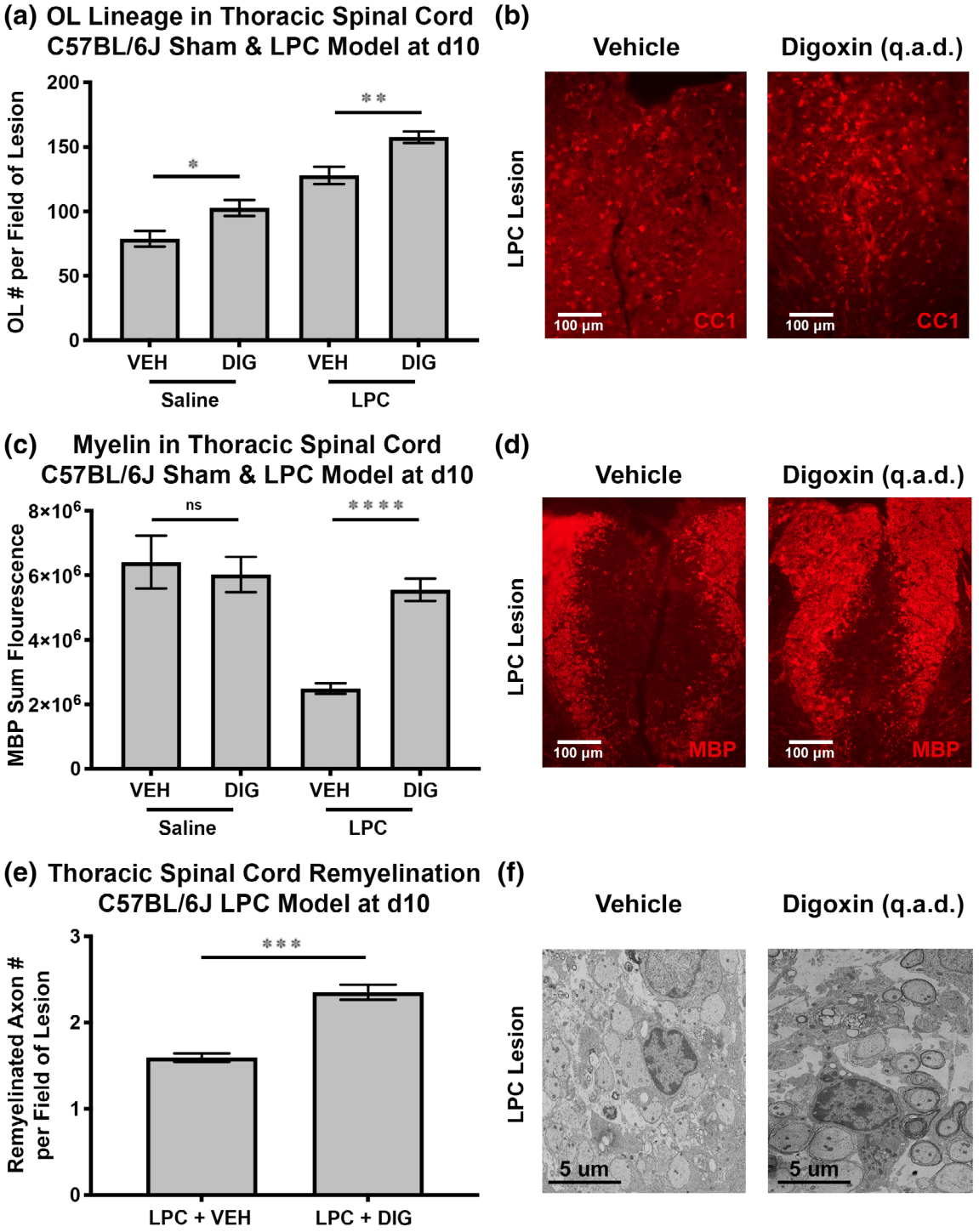

FIGURE 4 Digoxin promoted robust recovery of myelin in the LPC C57BL/6J mouse model of spinal cord focal demyelination/remyelination. Saline or LPC was injected into the thoracic spinal cord of 10-week-old female C57BL/6J mice on day 0. Performed blinded, mice were then treated i.p. with vehicle (VEH) or digoxin (DIG) 0.3 mg/kg qad on days 1–9 and sacrificed on day 10. Immunohistochemical quantitation of the average numbers of OLs ($CC1^+$) was determined for 3 mice/group (3–4 20× images per mouse) (a, b). Immunofluorescent staining of myelin basic protein was carried out with representative images for the treatment groups shown and MBP staining quantitated with results presented as fluorescence intensity ($n > 100$ values/mouse, $n = 3$ mice/group) (c, d). Remyelination was assessed by scanning EM of thoracic spinal cord at d10 post-LPC injection and the mean number of remyelinated axons were determined in $n > 12$ sections (10,000×, grid square area = 86.61 mm^2) of lesion (external and internal) evaluated for each mouse in $n = 4$ mice/group (e, f). (*$p < .05$, **$p < .01$, ***$p < .001$, ****$p < .0001$, ns, not significant). Extended data for Figure 4 is labeled as Figure S2.

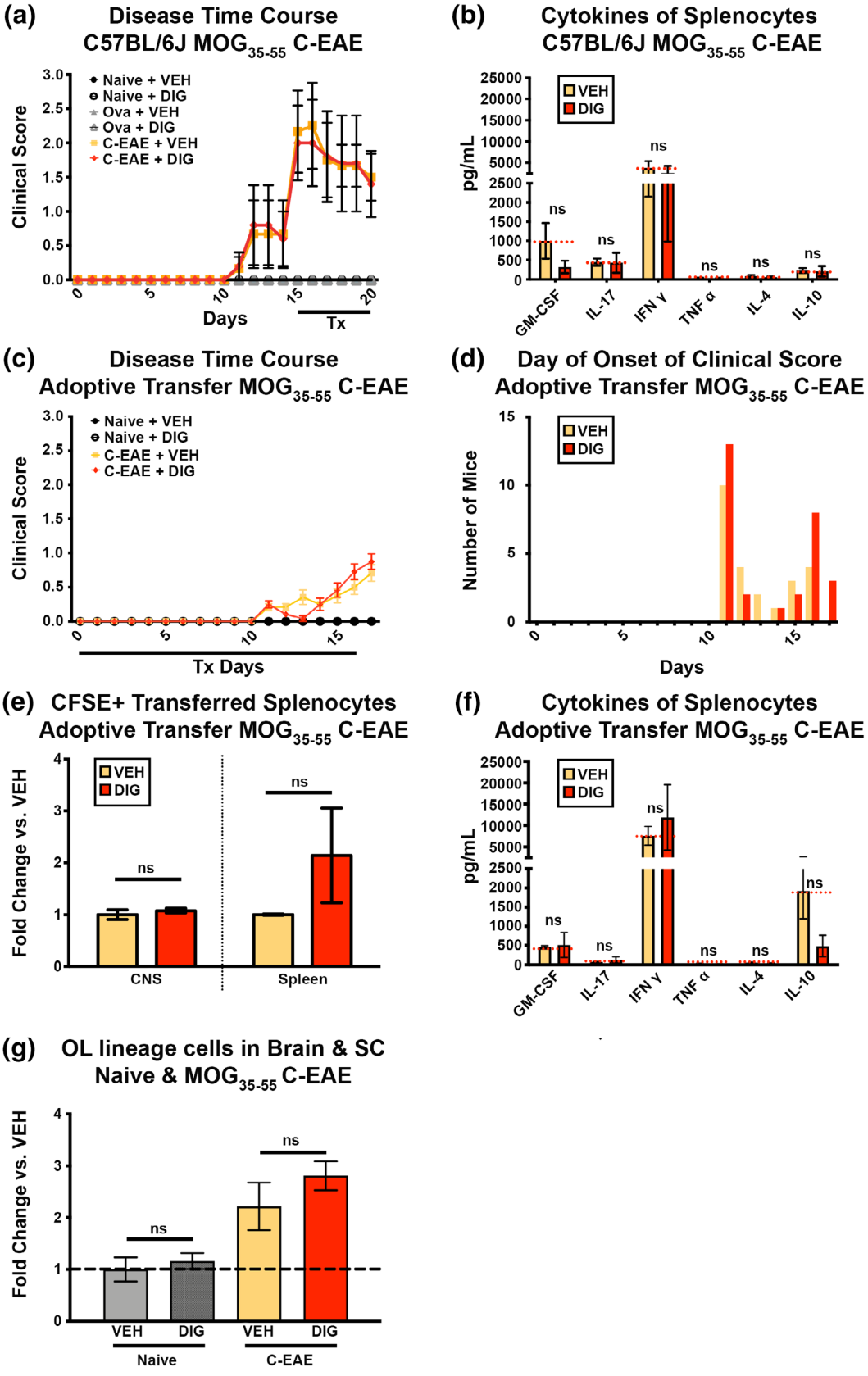

FIGURE 5 Legend on next page.

changes in myelination in vivo. We carried out a flow cytometric analysis of forebrains of naïve adult female C57BL/6J mice treated every other day (qad) with 0.3 mg/kg digoxin and showed that treatment promoted increased numbers of early OPCs at 2 weeks and a subsequent increase in OLs at 3 weeks, as determined by flow cytometry (Figure S1a). Digoxin treatment of naïve mice did not lead to a significant change in average g-ratio after 1, 2, or 3 weeks of treatment (Figure S1b). The significant change in small fibers at 1 week of digoxin treatment in naïve mice was transient and no longer present at 2 weeks (Figure S1c). We then asked if digoxin would more efficiently induce remyelination. We determined the effects of digoxin treatment of adult female C57BL/6J mice following cuprizone-induced demyelination, a well-characterized mouse model, used to investigate demyelination and remyelination (Praet et al., 2014). Flow cytometric analysis of the forebrains of digoxin-treated mice showed its ability to stimulate a robust increase of OL lineage cells after 3 weeks of dosing relative to vehicle-treated naïve control mice (Figure 3a). The data illustrated digoxin-induced differentiation of early OPCs to OLs over time (Figure S1a); indicated by a shift to an increase of OLs at 3 weeks post-treatment in both naïve control mice and the cuprizone induced model of demyelination (Figures S1a and 3a). Digoxin treatment of the cuprizone mouse model promoted an earlier reparative change in the cytoarchitecture of the corpus callosum as noted by changes in myelination (e.g., average g-ratio), due to cumulative changes in small and medium fibers one-week post-treatment (Figure 3b,c) as compared to vehicle treatment. The vehicle treated group had a significant change in average g-ratio, due to a robust change in small fibers and cumulatively with medium fibers, at 2 weeks. By 3 weeks, there was no significant difference in average g-ratio in digoxin versus vehicle treated mice (Figure 3b,c). Overall, this showed that treatment with digoxin did not lead to overcompensation resulting in hyper-myelination of axons in the forebrains of either naïve mice or the cuprizone mouse model, despite an overall increase in OL lineage cell number.

3.3 | Digoxin promoted robust recovery of myelin in the LPC C57BL/6J mouse model of spinal cord focal demyelination/remyelination

To assess the efficacy of digoxin to promote remyelination in the LPC-induced model of focal demyelination/remyelination, LPC lesions were induced in thoracic spinal cord of 10-week-old female C57BL/6J mice on day 0. The mice were then treated with vehicle or 0.3 mg/kg digoxin qad from days 1 to 9 and spinal cords harvested on day 10. Immunohistochemical analysis showed that digoxin treatment significantly increased the number of OLs (Figures 4a,b and S2a) in both saline "sham" and LPC spinal cord lesions. Digoxin treatment of mice induced a significant increase in the amount of myelin in thoracic cord LPC lesions as measured by fluorescence intensity of MBP staining (Figures 4c,d and S2b) and in the number of remyelinated axons as assessed by scanning EM (Figure 4e,f). Collectively, digoxin administration increased the number of OL lineage cells as well as robustly stimulate myelination through promotion of an earlier timeline of remyelination in the brain and the extent of remyelination in the spinal cord in the cuprizone and LPC chemically induced models of demyelination/remyelination, respectively (Figures 3 and 4).

3.4 | Immune cell function in vivo in female C57BL/6J C-EAE is not directly affected by digoxin

As we propose that treatment with antigen-specific tolerance immunotherapy combined with myelin repair/regenerative therapy is ideal for treatment of MS, we first tested if digoxin had inherent immunoregulatory properties. Therapeutic administration of 0.3 mg/kg digoxin beginning at the peak of active MOG_{35-55}/CFA-induced C-EAE in female C57BL/6J mice (days 15–20 post-immunization) failed to affect the clinical disease course (Figure 5a) or production of Th1 (IFN-γ and TNF-α), Th17 (IL-17 and GM-CSF), Th2 (IL-4) and regulatory (IL-10) cytokines elicited by in vitro stimulation of splenocytes upon re-activation with MOG_{35-55} (Figure 5b) when compared to responses from vehicle treated mice. Digoxin treatment also did not alter incidence, time of onset, or severity of clinical C-EAE disease symptoms in adult female C57BL/6J recipients of MOG_{35-55}-specific T cells adoptive transfer (Figure 5c,d). Furthermore, digoxin treatment did not alter homing of the transferred cells as there were similar numbers of donor CFSE-labeled cells in the CNS and spleens of the recipients (Figure 5e). Th1 (IFN-γ and TNF-α), Th17 (IL-17 and GM-CSF), Th2 (IL-4) and regulatory (IL-10) cytokine production by splenic T cells from the recipient mice in response to MOG_{35-55} were also not significantly different between vehicle- and digoxin-treated recipients (Figure 5f). Lastly, 5 days of digoxin treatment at the peak

FIGURE 5 Immune cell function in vivo in female C57BL/6J C-EAE is not directly affected by digoxin. 8-week-old female C57BL/6J mice remained naïve, or were primed with $OVA_{323-339}$, or primed with MOG_{35-55}, followed by treatment (Tx) i.p. with vehicle (VEH) or digoxin (DIG) 0.3 mg/kg qd for 5 days beginning at d15 post-priming. Clinical scores were assessed until d20 (a). At d20, splenocytes from the various groups ($n = 4$ mice/group) were re-activated in culture with MOG_{35-55} and cytokines in the culture supernatants were assessed for levels of the indicated cytokines using Luminex analysis (b). Female C57BL/6J recipient mice (8-weeks-old, $n = 24$ mice/group) received 3×10^6 in vitro peptide re-activated splenocytes labeled with CFSE from MOG_{35-55}-primed donor mice and were treated (Tx) i.p. with vehicle (VEH) or digoxin (DIG) 0.3 mg/kg qad from day 0–16; mean clinical scores (c) and day of onset of disease symptoms (d). At initial disease peak (day 17), mice were sacrificed and the numbers of donor MOG_{35-55}-specific $CFSE^+$ T cells in the brains and spleens of the recipient mice ($n = 6$ mice/group) were assessed (e). In addition, splenocytes from the recipient mice ($n = 6$ mice/group) were stimulated in culture with MOG_{35-55} and cytokine production in culture supernatants were assessed by Luminex assay (f). Flow cytometric analysis of forebrain/spinal cord OL lineage cells (pre-OL/OL, $O4^+$, measured as fold change vs. vehicle), of $n = 4$ mice/group from panel a with actively-induced C-EAE, was assessed at day 20 (g). (ns, not significant).

of active C-EAE in adult female C57BL/6J mice did not alter the total numbers of OL lineage cells in brain and spinal cord as compared to vehicle (Figure 5g). Collectively, these results indicated that short term digoxin treatment at 0.3 mg/kg appears not to be immunosuppressive or alter homing of activated T cells when used therapeutically in either active or adoptive transfer EAE.

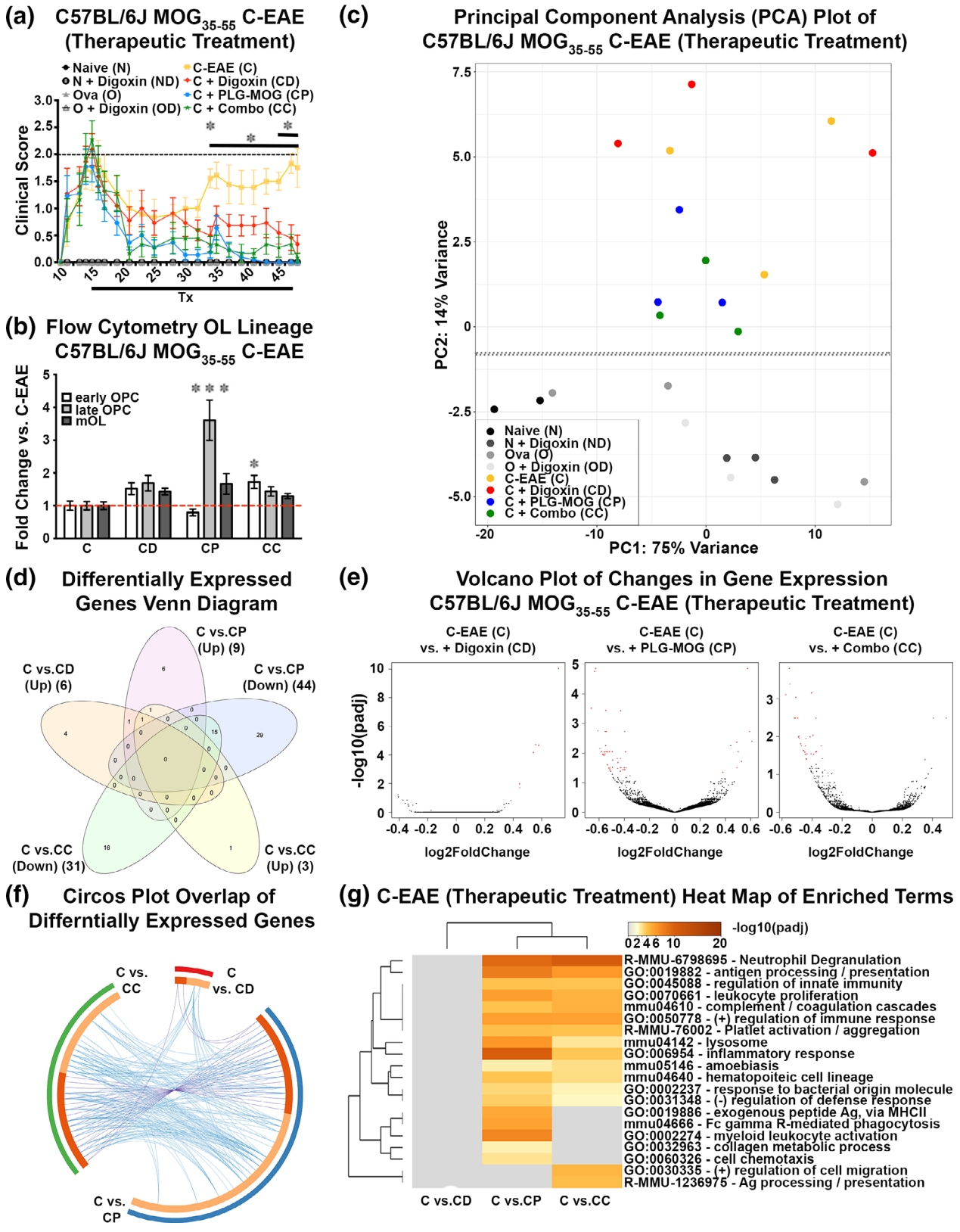

FIGURE 6 Legend on next page.

3.5 | Combined therapeutic treatment with digoxin and MOG_{35-55}-specific tolerance is additive for changes throughout the OL lineage in female C57BL/6J C-EAE

As both autoimmunity and neurodegeneration underlie MS pathogenesis, effective disease-modifying therapies need to both regulate the immune system and promote restoration of neuronal function, including remyelination. We thus tested the effects of combining tolerance induced by i.v. infusion of PLG nanoparticles encapsulating MOG_{35-55} peptide (PLG-MOG) and digoxin treatment for therapy of MOG_{35-55}/CFA-induced C-EAE. Adult female C57BL/6J mice at the peak of acute C-EAE (day 15) were tolerized with a single i.v. infusion of PLG-MOG nanoparticles and/or treated i.p. for the next 30 days with digoxin (0.3 mg/kg qad). PLG-MOG tolerance alone or in combination with digoxin treatment significantly reduced clinical paralytic symptoms of disease (i.e., clinical score) with mice showing sustained complete recovery 20–30 days post-treatment (Figure 6a). Flow cytometric analysis (measured as fold change of the percent of CNS cells in various C-EAE treatment groups compared to vehicle treatment) of OL lineage cells was performed on mouse forebrain and spinal cords at day 48 (6 mice per group) to determine if single and/or combination therapeutic treatment led to a recovery of the OL numbers and function. Interestingly, there was a significant increase in the late OPCs with PLG-MOG treatment alone that was not present in the mice treated with the drug combination and a smaller yet significant increase in the early OPCs in the mice treated with the combination of PLG-MOG and digoxin as compared to vehicle treated C-EAE (Figure 6b). To further evaluate the effects of tolerance immunotherapy in combination with digoxin, we carried out RNA sequencing of forebrain and spinal cord tissue from the various groups. PCA showed clustering within and between treatment groups (Figure 6c). PLG-MOG treatment, alone or in combination with digoxin, clustered tightly and with lower variance as compared to vehicle or digoxin alone. As noted by red dots in the Volcano plots, there were more significant differentially expressed genes in the PLG-MOG alone and combination treatment groups (Figure 6e). The Venn diagram showed the number of significant differentially expressed genes (up or down regulated) unique or shared in the therapeutically treated C-EAE mice as compared to vehicle treated (Figure 6d). The cumulative overlap of differentially expressed genes, of the same genes (purple lines) and functional overlap of different genes that fall into the same ontology (blue lines), are visualized in the Circos Plot (Figure 6f). A substantial portion of the differentially expressed genes were shared between the PLG-MOG combination and PLG-MOG alone groups, as indicated in the heatmap of enriched terms (Figure 6g). The top 20 pathways are mainly immune regulatory. Interestingly, all treatment groups have a subset of genes only significantly differentially expressed within those treatments (Figures 6d and S3).

Digoxin alone led to a diminished C-EAE clinical score during an extended 30-day time course of treatment (Figure 6a) as well as an increase in myelinating OLs (Figure 7a) relative to naïve mice. There was a significant increase in both early OPCs and myelinating OL in the combination treated C-EAE mice compared to naïve mice (Figure 7a). These changes in the OL lineage corresponded with significant increases in OL differentiation and maturation genes (e.g., *Nkx6-2*, *Gal3st1*) in C-EAE mice treated with digoxin alone or in combination. (Figure 7b). Of note, flow cytometric analysis of the OL lineage subsets at the completion of the treatments showed the predominant recovery of the disease-induced decrease of the pre-OL/OL population in mice treated with the combination of PLG-MOG and digoxin, but not with the individual treatments (Figure 7a).

Altogether, the additive effects in changes of OL differentiation and maturation gene expression could underlie the variation of significant changes in the immature and mature oligodendrocyte lineage cells across the single treatments as compared to combination therapy. Of note, there was a significant decrease in expression of the oligodendroglia-specific immunoproteasome subunit PSMB8 (*Psmb8*) in the combination treatment group as compared to vehicle treated C-EAE (Figure S3). Expression of *Psmb8* normalized to naïve

FIGURE 6 Combined therapeutic treatment with digoxin and MOG_{35-55}-specific tolerance ameliorated disease progression in female C57BL/6J C-EAE. 8-week-old female C57BL/6J mice remained naïve (N), or were primed with $OVA_{323-339}$ (O), or primed with MOG_{35-55} to induce C-EAE (C). At peak (d15), the MOG_{35-55} primed mice were treated (Tx) with vehicle (C) ($n = 9$) or treated with a single i.v. infusion PLG-MOG_{35-55} nanoparticles alone (CP) ($n = 11$), digoxin alone (CD) 0.3 mg/kg i.p. qad for 1 month through d46 ($n = 11$), or with the combination (CC) of PLG-MOG_{35-55} + digoxin ($n = 9$). Clinical scores were monitored until d47 (a): Compared to MOG primed + vehicle, there was a significant decrease in clinical score in d34 - d47 (PLG and combination) and at d34/d45-d47 (digoxin). During d35-d44, the digoxin cohort is not significantly different from the PLG or combo. On d47, forebrain and spinal cord tissue from perfused mice ($n = 3$–6 mice/group) was collected and processed for flow cytometric analysis of OL lineage cells (measured % CNS resident cells in treatment groups as a fold change compared to vehicle control MOG_{35-55} primed C-EAE) (b) and for RNASeq analysis (c–g). PCA shows variation within and between groups. Horizontal and vertical axis show two principal components that explain the greatest proportion (75% and 14%) of variation (c). Venn diagram displays the number of significantly differentially expressed genes in C57BL/6J MOG_{35} C-EAE (therapeutic treatment). Differential expression was determined using DESeq2 and the cutoff for determining significantly differentially expressed genes was an FDR-adjusted p-value <.05 (d). Volcano plots displays the differentially expressed genes in C57BL/6J MOG_{35} C-EAE (therapeutic treatment). The vertical axis (y-axis) corresponds to the FDR adjusted p-value ($-\log_{10}$), and the horizontal axis (x-axis) displays the fold change ($\log_2$). The red dots represent the significant genes. Positive x-values represent up-regulation and negative x-values represent down-regulation (e). Circos plot shows the overlap between gene lists, where purple curves link identical genes and blue curves link genes that belong to the same enriched ontology term. The inner circle represents gene lists, where hits are arranged along the arc. Genes that hit multiple lists are colored in dark orange, and genes unique to a list are shown in light orange (f). The heatmap shows the top 20 enriched clusters across C57BL/6J MOG_{35} C-EAE (therapeutic treatment), colored by significance, FDR adjusted p-value ($-$log10) (g). (*$p < .05$, **$p < .01$, ***$p < .001$). Extended data for Figure 6 is labeled as Figure S3.

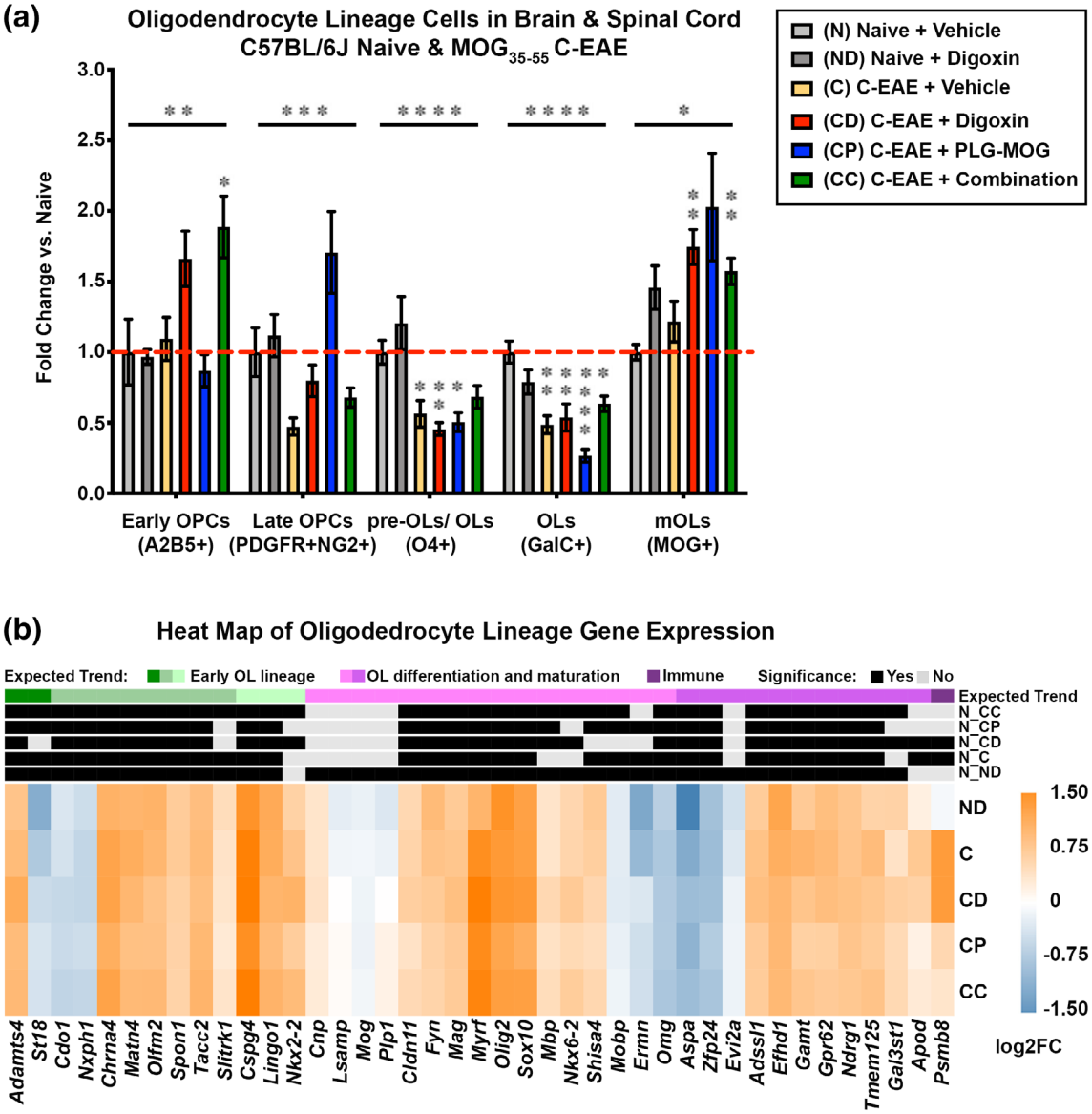

FIGURE 7 Combined therapeutic treatment with digoxin and MOG_{35-55}-specific tolerance was additive for changes throughout the OL lineage in female C57BL/6J C-EAE. Flow cytometric analysis of the OL lineage in female C57BL/6J forebrain and spinal cord (measured % CNS resident cells in treatment groups as a fold change compared to vehicle control naïve mice) was performed on following groups ($n = 3$–6 mice/group): Naïve + vehicle (N), Naïve + digoxin (ND), MOG_{35-55}-primed + vehicle (C), MOG_{35-55}-primed + digoxin (CD), MOG_{35-55}-primed + PLG-MOG (CP), and MOG_{35-55}-primed + combination (digoxin + PLG-MOG) (CC) treated mice (a). The heatmap shows relative expression of genes as fold change (log_2) based on expected trend at 1 month of treatment as compared to Naïve + vehicle. Orange color indicates relative upregulation, whereas blue indicated relative down regulation. Row annotations mark different expected trends, including; early OL lineage genes (green), OL differentiation and maturation genes (purple) as well as immune (dark purple). Genes that were significantly differentially expressed are marked in black (b). (*$p < .05$, **$p < .01$, ***$p < .001$, ****$p < .0001$).

levels when C-EAE mice were treated with PLG-MOG alone or in combination with digoxin, but not with digoxin treatment alone, providing additional evidence that digoxin did not appear to directly affect immune function (Figure 7b). Collectively, PLG-MOG tolerance therapy in combination with digoxin promoted changes throughout the OL lineage and induced complete recovery from clinical symptoms highlighting the importance of antigen-specific targeting the anti-myelin autoimmune response in combination with potential myelin protective and repair/regeneration drugs.

3.6 | Digoxin treatment does not alter astrocyte number or function in vitro or in vivo within models of demyelination/remyelination

Developmentally, OLs and astrocytes arise from a common glial progenitor. We thus tested the potential effects of digoxin on astrocytes in vitro and in vivo. There was no effect of Digoxin (in concentrations ranging from 0.01 to 10 ng/ml) on morphology of rat astrocytes cultured in serum free conditions for 24, 48, and 96 h.

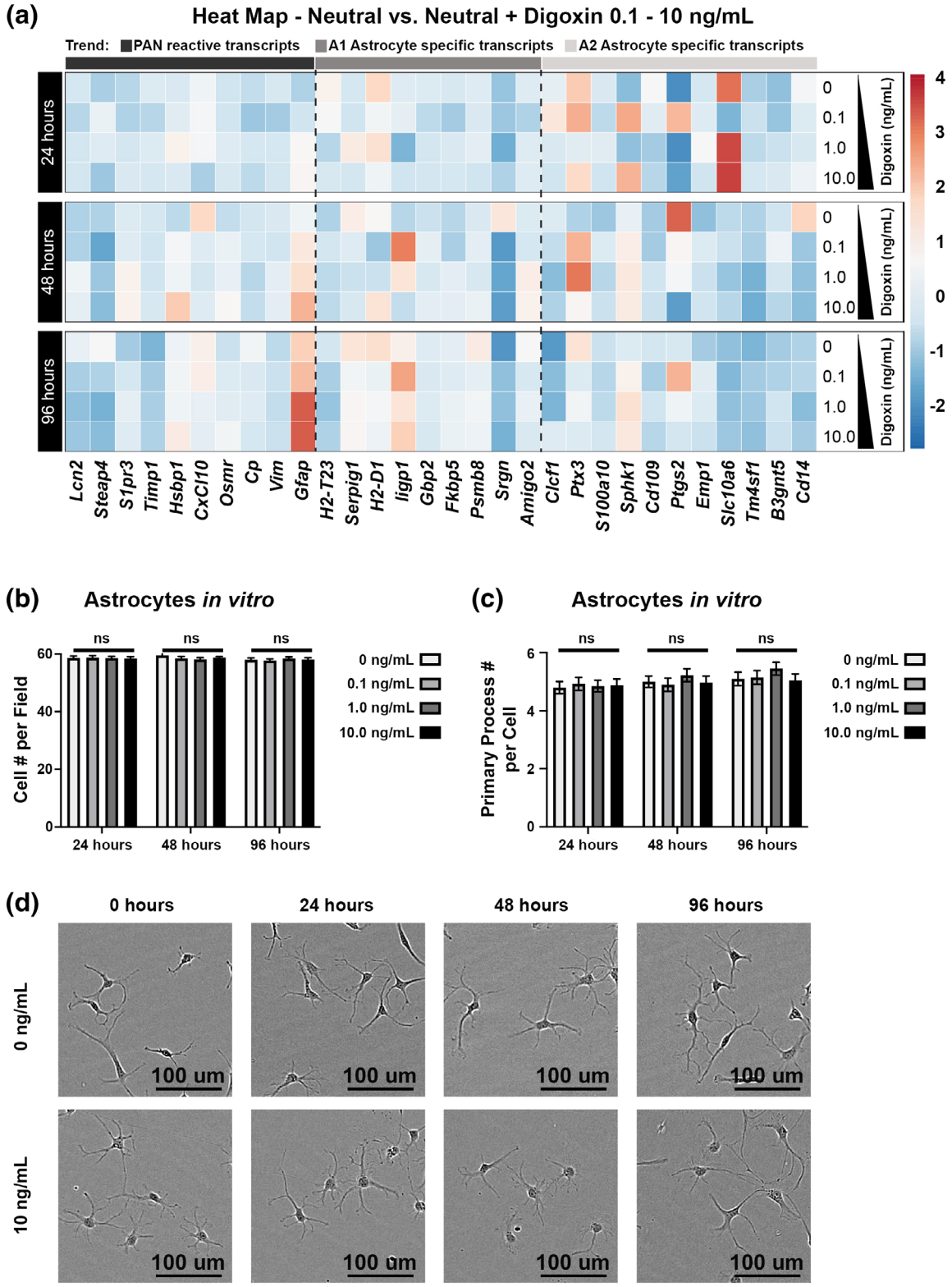

FIGURE 8 Digoxin treatment did not alter astrocyte number or function in vitro. After 1 week in culture, mixed male and female rat astrocytes were treated with digoxin (0.1, or 1.0, or 10.0 ng/ml) for 24 h (d1), 48 h (d2), and 96 h (d4). Total RNA was then extracted and microfluidic qPCR used to determine changes in astrocyte functional state. The heatmap shows relative expression of reactive astrocyte transcripts in digoxin-treated astrocytes compared to vehicle (a). Live phase contrast imaging of astrocytes was carried out at 20× with results presented as cell number per field (ROI) and average number of astrocyte primary processes per cell within each treatment group (b-d). (ns, not significant). Extended data for Figure 8 is labeled as Figure S4.

The cells maintained a processed, stellate appearance by phase imaging (Figure 8c/d) and the expression level of gene transcripts known to be involved in reactive astrocyte disease responses (Figure 8a). Additionally, there was not a significant change in the number of astrocytes, indicating that digoxin was neither toxic nor induced proliferation (Figure 8b). In vivo, Digoxin treatment did not lead to a significant difference in the total number of brain astrocytes in naïve or cuprizone fed mice treated for 1, 2, or 3 weeks (Figure S4a–c), nor in brain/SC astrocytes in naïve or C-EAE mice treated for 5 days (Figure S4d) or 1 month (Figure S4e). Interestingly, there was an overall decrease in brain/SC astrocytes in mice undergoing C-EAE at 1 month (as compared to naïve mice) that was reversed by treatment with both PLG-MOG and digoxin, but not with the individual treatments (Figure S4e). Additionally, Digoxin treatment did not lead to a significant difference in $GFAP^+$ astrocytes in the spinal cord as measured by fluorescence intensity in either saline "sham" lesioned or LPC lesioned mice (Figure S4f). Digoxin thus did not significantly alter the astrocyte transcriptomic phenotype in vitro nor astrocyte number in vivo in adult female C57BL/6J mice across several demyelinating disease models.

4 | DISCUSSION

MS is a CNS autoimmune disease characterized by demyelination, oligodendrocyte cell death and neurodegeneration (McFarland & Martin, 2007). Although there are nearly two dozen FDA-approved immune-based disease-modifying therapies (Tintore et al., 2019), there are currently no available therapies approved to promote myelin repair/regeneration or to prevent/ameliorate chronic neurodegeneration. The ideal treatment for MS would combine antigen-specific re-establishment of self-tolerance to myelin epitopes with drugs that protect from neurodegeneration and stimulate myelin repair/regeneration. In these studies, we demonstrated that digoxin promoted differentiation of the OL cell lineage in vitro as well as stimulated remyelination for preservation of axonal integrity in vivo in chemically-induced models of brain and spinal cord demyelination/remyelination as well as that digoxin can be combined with specific immune tolerance therapy to ameliorate disease progression and promote recovery of the OL lineage in EAE immune-mediated demyelination.

Regarding antigen-specific immunotherapy, our laboratory has developed a potent method for inducing self-tolerance which involves the i.v. administration of biodegradable carboxylated PLG nanoparticles encapsulating autoantigens (PLG-Ag) to induce T cell anergy and activate antigen-specific regulatory T cells (Tregs) (McCarthy et al., 2017). PLG-Ag treatment therapeutically ameliorates disease progression in mouse models of Th1/17- (e.g., EAE, T1D, celiac disease) and Th2 (e.g., egg allergy)-mediated diseases (Freitag et al., 2020; Getts et al., 2012; Getts et al., 2013; Hunter et al., 2014; Prasad et al., 2018; Smarr et al., 2016). Moreover, we have recently carried out a phase 1/2a clinical trial demonstrating that administration of PLG nanoparticles encapsulating gliadin safely and efficaciously induces tolerance in celiac disease patients undergoing oral gluten challenge resulting in a dramatic reduction in the number of gliadin-specific IFN-γ-producing T cells and protection from small bowel histopathology (Kelly et al., 2021). Relevant to MS immunotherapy, Cour Pharmaceuticals (www.courpharma.com), a company co-founded by Dr. Miller, is currently developing a clinical program testing the safety and efficacy of tolerance induced by PLG nanoparticles encapsulating a cocktail of encephalitogenic myelin peptide epitopes for treatment of early relapsing–remitting MS and neuromyelitis optica (NMO).

A K^+ channel blocker, 4-Aminopyridine (4-AP Ampyra), approved for treatment of walking impairment in MS by improving conduction velocity in demyelinated axons, has recently been shown to delay neuroaxonal loss (De Giglio et al., 2020; Dietrich et al., 2020). However, there are no approved therapies for myelin repair/regeneration. The Na^+/K^+ ATPase inhibitor, ouabain, had been previously studied in rat models of demyelination and in patients with MS; both studies reported improvements in conduction velocity of evoked potentials (Kaji et al., 1990; Kaji & Sumner, 1989). Making and maintaining myelin involves bioenergetic pathways; glycolysis is integral in myelin biosynthesis as well as extension of processes and oxidative phosphorylation for myelin maintenance (Bordone et al., 2019; Philips & Rothstein, 2017; Rinholm et al., 2011; Rosko et al., 2019; Simons & Nave, 2015), Na^+/K^+ ATPase inhibitors have been reported to alter bioenergetic pathways (i.e., level of aerobic glycolysis), and are likely to shift the level of bioenergetics in OPCs and OLs in naïve and stressed (i.e., disease state) conditions (Agathocleous et al., 2012; Parker & Hoffman, 1967; Rao et al., 2017; Rone et al., 2016; Yanes et al., 2010). The myelin-promoting capacity of the FDA-approved Na^+/K^+ ATPase inhibitor, digoxin, had previously been demonstrated in in vitro myelination screens (Lariosa-Willingham et al., 2016).

Due to the potency of digoxin in inducing myelination, the low cost, and ready availability, we initiated an investigation to determine how digoxin altered the transcriptional profile of OPCs to enhance their differentiation/maturation and to determine the capacity of digoxin to promote myelin regeneration in vivo. We demonstrate that digoxin promoted a transcriptional profile consistent with differentiation and maturation of OPCs in vitro and promoted remyelination in vivo in the cuprizone- and LPC models of demyelination/remyelination, and when combined with PLG-Ag tolerance promoted recovery of the OL lineage and improved clinical scores throughout the course of the Th1/Th17-mediated model of MOG_{35-55}-induced C-EAE.

We first examined the transcriptional profile induced in digoxin-treated OPCs in vitro and demonstrated significant down-regulation of early OL lineage genes and up-regulation OL differentiation/maturation genes (Figures 1 and 2). There was strong overlap in genes differentially expressed and enriched in OPCs stimulated with 10 ng/ml digoxin (ND10) and those cultured with the differentiation (T3) control (Figures 1 and 2). Interestingly, there were notable differences in the levels of expression of genes cumulatively influencing OL differentiation (Elbaz & Popko, 2019) induced by digoxin compared to T3 (Figures 1 and 2). Of note, there was no change in the total number of $DAPI^+$ cells; the increase in MBP MFI in the positive control (T3) was due to an increase in MBP per cell, however, the increase in MBP MFI in digoxin treated cells was due to an increase in the total

MBP^+ cell number and %$MBP/DAPI^+$ as compared to vehicle treated. This suggests that digoxin does not promote overproduction of myelin per cell in vitro.

We noted that brain myelin thickness (average g-ratio) was not significantly altered in naïve control female C57BL/6J mice treated with digoxin for 1, 2, or 3 weeks despite an increase in OPCs then OLs over weeks 2 and 3, respectively (Figure S1). Initial testing of the ability of digoxin administration to enhance re-myelination in the corpus callosum of mice undergoing cuprizone-induced demyelination showed that treatment significantly impacted myelin regeneration at earlier time points as compared to the natural recovery that occurs in the -cuprizone-induced demyelination model with vehicle treatment (Figure 3). Interestingly, the initial changes in myelin regeneration were present prior to a significant change in oligodendrocyte cell number. This suggests that digoxin treatment either stimulates myelination of axons by restabilizing OL function in existing mature cells and/or promoting the natural turnover of dysfunctional OL's and maturation of the OPC population. Of note, there was no overcompensation (e.g., hyper-myelination of axons) in the forebrains of naïve mice nor in the cuprizone mouse model, despite induced changes in the OL cell lineage.

Similarly, we found more robust induction of remyelination in digoxin treated mice following induction of focal demyelinating LPC lesions in the spinal cord (Figure 4). There was an increase in OL number correlated with a recovery of mean fluorescence intensity of MBP and a significant increase in the number of myelinated axons per lesion area in digoxin treated mice. Of note, there was no change in mean fluorescence intensity of MBP in digoxin-treated saline "sham" lesion mice despite an increase in number of mature OLs, additionally highlighting that digoxin treatment does not cause over-production of spinal cord myelin (Figures 4 and S2). Collectively, these in vivo experiments demonstrate the ability of digoxin to promote myelin regeneration and maintenance of axon integrity in chemically-induced CNS models of demyelination/remyelination.

Most relevant to MS, we show that digoxin treatment promoted OL cell lineage number and functional recovery in the enhanced inflammatory environment present in the T cell-mediated MOG_{35-55}-induced C-EAE model of the disease. Short-term digoxin monotherapy beginning at the peak of actively-induced C-EAE did not alter the course of clinical disease, nor significantly alter the number of brain and spinal cord OLs or Th1/17 inflammatory cytokine responses of splenocytes upon recall MOG_{35-55} stimulation (Figure 5). Similarly, digoxin treatment did not alter clinical disease symptoms, time of onset, or the levels of proliferative or cytokine responses of adoptive recipients of MOG_{35-55}-activated encephalitogenic T cells (Figure 5). Collectively, these results indicated that digoxin alone at 0.3 mg/kg has no apparent direct effects on induction or effector function of encephalitogenic Th1/17 cells in vivo and critically that myelin repair/regenerative therapy with digoxin has little efficacy as a short-term monotherapy in C-EAE immune-mediated demyelinating disease.

As indicated previously, both immune-mediated demyelination and failure to repair/regenerate myelin underly the pathogenesis of MS. We thus hypothesized that the combining digoxin treatment with PLG-MOG_{35-55} tolerance induction (to ameliorate ongoing autoimmune CNS destruction) would promote better restoration of CNS function. The results indicated more effective and sustained recovery of OL lineage cells and clinical symptoms in mice with C-EAE treated with the combination of MOG_{35-55}-PLG tolerance and digoxin beginning at the peak of acute disease (Figure 6).

Digoxin alone and combined therapy increased expression of OL differentiation genes (e.g., *Nkx6-2*, *Gal3st1*) in the brain and spinal cord of C-EAE mice. Interestingly, there was a significant decrease in the expression of *Psmb8*, which encodes the immunoproteasome subunit PSMB8 expressed on oligodendroglia in human demyelinated brain lesions (Kirby et al., 2019), in C-EAE mice treated with tolerance alone or in combination. Digoxin and PLG are ideal for combination therapy because of their independent mechanisms of action, ameliorating different steps of the disease process and mutual potentiating effects. Combined therapy was characterized by a significant increase in both OPCs and myelinating OLs as well as by reversal of the disease-induced decrease of intermediate OLs which was not observed with either individual treatment (Figures 6 and 7). Collectively, these results indicated that restoring the OL lineage is best achieved when digoxin treatment was combined with selective targeting of the myelin-specific autoimmune response, with the caveat that our analysis of the glial cell lineage is by necessity limited to snap shots in time. It will be interesting in future experiments to utilize in vitro systems to test specific cell populations under stressors to mimic in vivo model microenvironments. In the C-EAE model, treatment with digoxin at peak diminished clinical score at +30 days correlating with an increase in OLs (as compared to Naïve mice). Therapeutic treatment with PLG alone or in combination diminished clinical score at +20 days. Initial lower clinical scores could be due to maintenance of conduction velocity through demyelinated axons. However, only the combination therapy recovers the intermediate pre-OL/OL population; sustaining an available pool for OL turnover to limit damage and restore axonal function.

Notably digoxin treatment did not alter astrocytes number or phenotype in vitro (Figure 8), nor astrocyte number in vivo within the various disease models (Figure S4). Interestingly, compared to naïve mice, there was an overall decrease in astrocyte number in the brain and spinal cord of C-EAE mice one-month post-C-EAE induction that was recovered only upon treatment with digoxin combined with PLG-MOG_{35-55}, tolerance (Figures 8 and S4). This may be due, in part, to a sustained increase in early glial progenitors in mice treated with both digoxin and PLG-MOG_{35-55} but not with the individual treatments (Figure 7). Astrocytic scar formation is a major pathological process in MS that impedes effective tissue repair, remyelination, and axonal regeneration as well as therapeutic targeting of lesions. It will be interesting in future experiments to further observe the effects of digoxin on astrocytes in neurodegenerative conditions for potential of an anti-scaring treatment strategy that can be used in conjunction with immunotherapies and as well as other remyelinating drugs with the goal to permit and enhance the reparative processes in the CNS.

In summary, our results show that combining targeted myelin tolerance immunotherapy, thus avoiding the serious side effects of immunosuppressive therapies, with myelin repair/regenerative therapy is highly effective in ameliorating C-EAE, exceeding the

effects of either therapy alone. These findings provide critical proof-of-concept support for testing these combination therapies in MS patients. We are planning a phase 1 trial of Digoxin in MS patients with currently approved disease-modifying therapies. Due to fact that digoxin is a long-standing FDA-approved medication and that PLG-Ag tolerance has recently demonstrated safety and efficacy in phase 1/2a clinical testing in patients with celiac disease (Kelly et al., 2021), there is promise that this combination could soon undergo clinical testing.

AUTHOR CONTRIBUTIONS

Conceived and designed the experiments: Haley E. Titus, Andrew P. Robinson, Joseph R. Podojil, Stephen D. Miller, Roumen Balabanov, Huan Xu, Brian Popko, Molly Karl, Robert H. Miller, Shane A. Liddelow. Performed the experiments/collected data: Haley E. Titus, Andrew P. Robinson, Huan Xu, Yanan Chen, Valerie Eaton, Ming Yi Chiang, Molly Karl, Eric D. Garrison, Indigo V. L. Rose. Analyzed the data: Haley E. Titus, Huan Xu, Priyam A. Patel, Yanan Chen, Damiano Fantini, Stephen D. Miller, Molly Karl, Robert H. Miller, Indigo V. L. Rose, Shane A. Liddelow. Wrote the paper: Haley E. Titus, Stephen D. Miller. Edited the paper: Haley E. Titus, Stephen D. Miller, Roumen Balabanov, Huan Xu, Brian Popko, Molly Karl, Robert H. Miller, Shane A. Liddelow.

ACKNOWLEDGMENTS

We acknowledge the Robert H. Lurie Comprehensive Cancer Center Flow Cytometry Core Facility for the assistance of data acquisition, the Northwestern University Center for Advanced Microscopy for the assistance of data acquisition, the Northwestern University NUSeq Core Facility for the assistance of data acquisition, the Northwestern University Quantitative Data Science Core for the assistance of data acquisition and analysis, and the George Washington University Nanofabrication and Imaging Center for the assistance of data acquisition. We thank Miller laboratory members for all of their support and insight. This work was supported by NIH Grants R01 NS099334 and R21 AI142059 (Miller, S.D., PI), National Multiple Sclerosis Society (NMSS) Post-Doctoral Fellowship FG 20125-A-1 (Titus, H.E., PI), R01 NS109372 (BP), NMSS RG-1807-32005 (BP). We also acknowledge the Myelin Repair Foundation (SDM, BP and RM), the Johnnie Walker's MS Foundation (SDM), the David & Amy Fulton Foundation (SDM), and the Crammer Family Foundation (SDM), Dr. Miriam and Sheldon G. Adelson Medical Research Foundation (BP), the Rampy MS Research Foundation (BP), the NYU School of Medicine (SAL), The Blas Frangione Foundation (SAL), the Cure Alzheimer's Fund (SAL), anonymous donors (SAL), and the Novartis Institute for Biomedical Research (SAL). [Correction added on August 17, 2022, after first online publication: "The Myelin Repair Foundation (SDM, BP and RM)" has been included to the Acknowledgement section]

CONFLICTS OF INTEREST

Shane A. Liddelow is an academic founder of AstronauTx Ltd. Stephen D. Miller is an academic co-founder, scientific advisory board member, paid consultant, and grantee of Cour Pharmaceuticals; scientific advisory board member and grantee of NextCure, Inc., scientific advisory board member of Takeda Pharmaceuticals and Myeloid Therapeutics. Roumen Balabanov has received honorariums and research support from Biogen, Genzyme-Sanofi, Genentech, and Alexion.

DATA AVAILABILITY STATEMENT

RNA Seq data will be made publicly available through deposit on the NIH NCBI Gene Expression Omnibus (GEO).

ORCID

Haley E. Titus https://orcid.org/0000-0002-2327-9791
Huan Xu https://orcid.org/0000-0003-1544-2015
Andrew P. Robinson https://orcid.org/0000-0002-1867-5634
Priyam A. Patel https://orcid.org/0000-0002-9433-5017
Yanan Chen https://orcid.org/0000-0001-5510-231X
Damiano Fantini https://orcid.org/0000-0001-7858-0170
Molly Karl https://orcid.org/0000-0002-8520-7240
Eric D. Garrison https://orcid.org/0000-0002-2916-5752
Indigo V. L. Rose https://orcid.org/0000-0003-0491-1269
Ming Yi Chiang https://orcid.org/0000-0003-0959-2439
Joseph R. Podojil https://orcid.org/0000-0002-5818-8515
Roumen Balabanov https://orcid.org/0000-0002-7235-2078
Shane A. Liddelow https://orcid.org/0000-0002-0840-1437
Robert H. Miller https://orcid.org/0000-0001-9050-4154
Brian Popko https://orcid.org/0000-0001-9948-2553
Stephen D. Miller https://orcid.org/0000-0002-9556-0718

REFERENCES

Agathocleous, M., Love, N. K., Randlett, O., Harris, J. J., Liu, J., Murray, A. J., & Harris, W. A. (2012). Metabolic differentiation in the embryonic retina. *Nature Cell Biology*, *14*(8), 859–864. https://doi.org/10.1038/ncb2531

Anders, S., Pyl, P. T., & Huber, W. (2015). HTSeq–a python framework to work with high-throughput sequencing data. *Bioinformatics*, *31*(2), 166–169. https://doi.org/10.1093/bioinformatics/btu638

Andrews, S. (2010). FastQC: A quality control tool for high throughput sequence data. http://www.bioinformatics.babraham.ac.uk/projects/fastqc.

Bordone, M. P., Salman, M. M., Titus, H. E., Amini, E., Andersen, J. V., Chakraborti, B., Diuba, A. V., Dubouskaya, T. G., Ehrke, E., Espindola de Freitas, A., Braga de Freitas, G., Gonçalves, R. A., Gupta, D., Gupta, R., Ha, S. R., Hemming, I. A., Jaggar, M., Jakobsen, E., Kumari, P., Lakkappa, N., & Seidenbecher, C. I. (2019). The energetic brain - A review from students to students. *Journal of Neurochemistry*, *151*(2), 139–165. https://doi.org/10.1111/jnc.14829

Caprariello, A. V., Batt, C. E., Zippe, I., Romito-DiGiacomo, R. R., Karl, M., & Miller, R. H. (2015). Apoptosis of oligodendrocytes during early development delays myelination and impairs subsequent responses to demyelination. *The Journal of Neuroscience*, *35*(41), 14031–14041. https://doi.org/10.1523/JNEUROSCI.1706-15.2015

De Giglio, L., Cortese, F., & Pennisi, E. M. (2020). Aminopiridines in the treatment of multiple sclerosis and other neurological disorders. *Neurodegenerative Disease Management*, *10*(6), 409–423. https://doi.org/10.2217/nmt-2020-0018

Deshmukh, V. A., Tardif, V., Lyssiotis, C. A., Green, C. C., Kerman, B., Kim, H. J., Padmanabhan, K., Swoboda, J. G., Ahmad, I., Kondo, T., Gage, F. H., Theofilopoulos, A. N., Lawson, B. R., Schultz, P. G., & Lairson, L. L. (2013). A regenerative approach to the treatment of multiple sclerosis. *Nature*, *502*(7471), 327–332. https://doi.org/10.1038/nature12647

Dietrich, M., Koska, V., Hecker, C., Göttle, P., Hilla, A. M., Heskamp, A., Lepka, K., Issberner, A., Hallenberger, A., Baksmeier, C., Steckel, J., Balk, L., Knier, B., Korn, T., Havla, J., Martínez-Lapiscina, E. H., Solà-Valls, N., Manogaran, P., Olbert, E. D., Schippling, S., & Albrecht, P. (2020). Protective effects of 4-aminopyridine in experimental optic neuritis and multiple sclerosis. *Brain*, *143*(4), 1127–1142. https://doi.org/10.1093/brain/awaa062

Dobin, A., Davis, C. A., Schlesinger, F., Drenkow, J., Zaleski, C., Jha, S., Batut, P., Chaisson, M., & Gingeras, T. R. (2013). STAR: ultrafast universal RNA-seq aligner. *Bioinformatics*, *29*(1), 15–21. https://doi.org/10.1093/bioinformatics/bts635

Elbaz, B., & Popko, B. (2019). Molecular control of oligodendrocyte development. *Trends in Neurosciences*, *42*(4), 263–277. https://doi.org/10.1016/j.tins.2019.01.002

Emery, B., & Dugas, J. C. (2013). Purification of oligodendrocyte lineage cells from mouse cortices by immunopanning. *Cold Spring Harbor Protocols*, *2013*(9), 854–868. https://doi.org/10.1101/pdb.prot073973

Ewels, P., Magnusson, M., Lundin, S., & Kaller, M. (2016). MultiQC: Summarize analysis results for multiple tools and samples in a single report. *Bioinformatics*, *32*(19), 3047–3048. https://doi.org/10.1093/bioinformatics/btw354

Foo, L. C., Allen, N. J., Bushong, E. A., Ventura, P. B., Chung, W. S., Zhou, L., Cahoy, J. D., Daneman, R., Zong, H., Ellisman, M. H., & Barres, B. A. (2011). Development of a method for the purification and culture of rodent astrocytes. *Neuron*, *71*(5), 799–811. https://doi.org/10.1016/j.neuron.2011.07.022

Freitag, T. L., Podojil, J. R., Pearson, R. M., Fokta, F. J., Sahl, C., Messing, M., Andersson, L. C., Leskinen, K., Saavalainen, P., Hoover, L. I., Huang, K., Phippard, D., Maleki, S., King, N., Shea, L. D., Miller, S. D., Meri, S. K., & Getts, D. R. (2020). Gliadin nanoparticles induce immune tolerance to gliadin in mouse models of celiac disease. *Gastroenterology*, *158*(6), 1667–1681. https://doi.org/10.1053/j.gastro.2020.01.045

Getts, D. R., Martin, A. J., McCarthy, D. P., Terry, R. L., Hunter, Z. N., Yap, W. T., Getts, M. T., Pleiss, M., Luo, X., King, N. J., Shea, L. D., & Miller, S. D. (2012). Microparticles bearing encephalitogenic peptides induce T-cell tolerance and ameliorate experimental autoimmune encephalomyelitis. *Nature Biotechnology*, *30*(12), 1217–1224. https://doi.org/10.1038/nbt.2434

Getts, D. R., McCarthy, D. P., & Miller, S. D. (2013). Exploiting apoptosis for therapeutic tolerance induction. *Journal of Immunology*, *191*(11), 5341–5346. https://doi.org/10.4049/jimmunol.1302070

Glass, C. K., Saijo, K., Winner, B., Marchetto, M. C., & Gage, F. H. (2010). Mechanisms underlying inflammation in neurodegeneration. *Cell*, *140*(6), 918–934. https://doi.org/10.1016/j.cell.2010.02.016

Heberle, H., Meirelles, G. V., da Silva, F. R., Telles, G. P., & Minghim, R. (2015). InteractiVenn: A web-based tool for the analysis of sets through Venn diagrams. *BMC Bioinformatics*, *16*, 169. https://doi.org/10.1186/s12859-015-0611-3

Hunter, Z., McCarthy, D. P., Yap, W. T., Harp, C. T., Getts, D. R., Shea, L. D., & Miller, S. D. (2014). A biodegradable nanoparticle platform for the induction of antigen-specific immune tolerance for treatment of autoimmune disease. *ACS Nano*, *8*(3), 2148–2160. https://doi.org/10.1021/nn405033r

Kaji, R., Happel, L., & Sumner, A. J. (1990). Effect of digitalis on clinical symptoms and conduction variables in patients with multiple sclerosis. *Annals of Neurology*, *28*(4), 582–584. https://doi.org/10.1002/ana.410280419

Kaji, R., & Sumner, A. J. (1989). Effect of digitalis on central demyelinative conduction block in vivo. *Annals of Neurology*, *25*(2), 159–165. https://doi.org/10.1002/ana.410250209

Kaji, R., Suzumura, A., & Sumner, A. J. (1988). Physiological consequences of antiserum-mediated experimental demyelination in CNS. *Brain*, *111*(3), 675–694. https://doi.org/10.1093/brain/111.3.675

Kelly, C. P., Murray, J. A., Leffler, D. A., Getts, D. R., Bledsoe, A. C., Smithson, G., First, M. R., Morris, A., Boyne, M., Elhofy, A., Wu, T. T., Podojil, J. R., Miller, S. D., & TAK-101 Study Group (2021). TAK-101 nanoparticles induced gluten-specific tolerance in celiac disease: A randomized, double-blind, placebo-controlled study. *Gastroenterology* 161(1), 66-80 e68. https://doi.org/10.1053/j.gastro.2021.03.014

Keough, M. B., Jensen, S. K., & Yong, V. W. (2015). Experimental demyelination and remyelination of murine spinal cord by focal injection of lysolecithin. *Journal of Visualized Experiments*, (97), 52679. https://doi.org/10.3791/52679

Kirby, L., Jin, J., Cardona, J. G., Smith, M. D., Martin, K. A., Wang, J., Strasburger, H., Herbst, L., Alexis, M., Karnell, J., Davidson, T., Dutta, R., Goverman, J., Bergles, D., & Calabresi, P. A. (2019). Oligodendrocyte precursor cells present antigen and are cytotoxic targets in inflammatory demyelination. *Nature Communications*, *10*(1), 3887. https://doi.org/10.1038/s41467-019-11638-3

Lariosa-Willingham, K. D., Rosler, E. S., Tung, J. S., Dugas, J. C., Collins, T. L., & Leonoudakis, D. (2016). Development of a central nervous system axonal myelination assay for high throughput screening. *BMC Neuroscience*, *17*, 16. https://doi.org/10.1186/s12868-016-0250-2

Laursen, M., Gregersen, J. L., Yatime, L., Nissen, P., & Fedosova, N. U. (2015). Structures and characterization of digoxin- and bufalin-bound Na+,K+-ATPase compared with the ouabain-bound complex. *Proceedings of the National Academy of Sciences of the United States of America*, *112*(6), 1755–1760. https://doi.org/10.1073/pnas.1422997112

Liddelow, S. A., Guttenplan, K. A., Clarke, L. E., Bennett, F. C., Bohlen, C. J., Schirmer, L., Bennett, M. L., Münch, A. E., Chung, W. S., Peterson, T. C., Wilton, D. K., Frouin, A., Napier, B. A., Panicker, N., Kumar, M., Buckwalter, M. S., Rowitch, D. H., Dawson, V. L., Dawson, T. M., Stevens, B., … Barres, B. A. (2017). Neurotoxic reactive astrocytes are induced by activated microglia. *Nature*, *541*(7638), 481–487. https://doi.org/10.1038/nature21029

Love, M. I., Huber, W., & Anders, S. (2014). Moderated estimation of fold change and dispersion for RNA-seq data with DESeq2. *Genome Biology*, *15*(12), 550. https://doi.org/10.1186/s13059-014-0550-8

Luo, X., Miller, S. D., & Shea, L. D. (2016). Immune tolerance for autoimmune disease and cell transplantation. *Annual Review of Biomedical Engineering*, *18*, 181–205. https://doi.org/10.1146/annurev-bioeng-110315-020137

Lutterotti, A., Yousef, S., Sputtek, A., Stürner, K. H., Stellmann, J. P., Breiden, P., Reinhardt, S., Schulze, C., Bester, M., Heesen, C., Schippling, S., Miller, S. D., Sospedra, M., & Martin, R. (2013). Antigen-specific tolerance by autologous myelin peptide-coupled cells: A phase 1 trial in multiple sclerosis. *Science Translational Medicine*, *5*, 188ra75. https://doi.org/10.1126/scitranslmed.3006168

McCarthy, D. P., Hunter, Z. N., Chackerian, B., Shea, L. D., & Miller, S. D. (2014). Targeted immunomodulation using antigen-conjugated nanoparticles. *Wiley Interdisciplinary Reviews. Nanomedicine and Nanobiotechnology*, *6*(3), 298–315. https://doi.org/10.1002/wnan.1263

McCarthy, D. P., Yap, J. W., Harp, C. T., Song, W. K., Chen, J., Pearson, R. M., Miller, S. D., & Shea, L. D. (2017). An antigen-encapsulating nanoparticle platform for TH1/17 immune tolerance therapy. *Nanomedicine*, *13*(1), 191–200. https://doi.org/10.1016/j.nano.2016.09.007

McFarland, H. F., & Martin, R. (2007). Multiple sclerosis: A complicated picture of autoimmunity. *Nature Immunology*, *8*(9), 913–919. https://doi.org/10.1038/ni1507

Mei, F., Fancy, S., Shen, Y. A., Niu, J., Zhao, C., Presley, B., Miao, E., Lee, S., Mayoral, S. R., Redmond, S. A., Etxeberria, A., Xiao, L., Franklin, R., Green, A., Hauser, S. L., & Chan, J. R. (2014). Micropillar arrays as a high-throughput screening platform for therapeutics in multiple sclerosis. *Nature Medicine*, *20*(8), 954–960. https://doi.org/10.1038/nm.3618

Najm, F. J., Madhavan, M., Zaremba, A., Shick, E., Karl, R. T., Factor, D. C., Miller, T. E., Nevin, Z. S., Kantor, C., Sargent, A., Quick, K. L., Schlatzer, D. M., Tang, H., Papoian, R., Brimacombe, K. R., Shen, M., Boxer, M. B.,

Jadhav, A., Robinson, A. P., Podojil, J. R., & Tesar, P. J. (2015). Drug-based modulation of endogenous stem cells promotes functional remyelination in vivo. *Nature*, *522*(7555), 216–220. https://doi.org/10.1038/nature14335

Parker, J. C., & Hoffman, J. F. (1967). The role of membrane phosphoglycerate kinase in the control of glycolytic rate by active cation transport in human red blood cells. *The Journal of General Physiology*, *50*(4), 893–916. https://doi.org/10.1085/jgp.50.4.893

Pearson, R. M., Casey, L. M., Hughes, K. R., Miller, S. D., & Shea, L. D. (2017). In vivo reprogramming of immune cells: Technologies for induction of antigen-specific tolerance. *Advanced Drug Delivery Reviews*, *114*, 240–255. https://doi.org/10.1016/j.addr.2017.04.005

Pearson, R. M., Podojil, J. R., Shea, L. D., King, N. J. C., Miller, S. D., & Getts, D. R. (2019). Overcoming challenges in treating autoimmunity: Development of tolerogenic immune-modifying nanoparticles. *Nanomedicine*, *18*, 282–291. https://doi.org/10.1016/j.nano.2018.10.001

Pfaffl, M. W. (2001). A new mathematical model for relative quantification in real-time RT-PCR. *Nucleic Acids Research*, *29*(9), e45. https://doi.org/10.1093/nar/29.9.e45

Philips, T., & Rothstein, J. D. (2017). Oligodendroglia: Metabolic supporters of neurons. *The Journal of Clinical Investigation*, *127*(9), 3271–3280. https://doi.org/10.1172/JCI90610

Praet, J., Guglielmetti, C., Berneman, Z., Van der Linden, A., & Ponsaerts, P. (2014). Cellular and molecular neuropathology of the cuprizone mouse model: Clinical relevance for multiple sclerosis. *Neuroscience and Biobehavioral Reviews*, *47*, 485–505. https://doi.org/10.1016/j.neubiorev.2014.10.004

Prasad, S., Neef, T., Xu, D., Podojil, J. R., Getts, D. R., Shea, L. D., & Miller, S. D. (2018). Tolerogenic ag-PLG nanoparticles induce tregs to suppress activated diabetogenic CD4 and CD8 T cells. *Journal of Autoimmunity*, *89*, 112–124. https://doi.org/10.1016/j.jaut.2017.12.010

Prinz, M., & Kalinke, U. (2010). New lessons about old molecules: How type I interferons shape Th1/Th17-mediated autoimmunity in the CNS. *Trends in Molecular Medicine*, *16*(8), 379–386. https://doi.org/10.1016/j.molmed.2010.06.001

Rao, V., Khan, D., Cui, Q. L., Fuh, S. C., Hossain, S., Almazan, G., Multhaup, G., Healy, L. M., Kennedy, T. E., & Antel, J. P. (2017). Distinct age and differentiation-state dependent metabolic profiles of oligodendrocytes under optimal and stress conditions. *PLoS One*, *12*(8), e0182372. https://doi.org/10.1371/journal.pone.0182372

Rinholm, J. E., Hamilton, N. B., Kessaris, N., Richardson, W. D., Bergersen, L. H., & Attwell, D. (2011). Regulation of oligodendrocyte development and myelination by glucose and lactate. *The Journal of Neuroscience*, *31*(2), 538–548. https://doi.org/10.1523/JNEUROSCI.3516-10.2011

Robinson, A. P., Rodgers, J. M., Goings, G. E., & Miller, S. D. (2014). Characterization of oligodendroglial populations in mouse demyelinating disease using flow cytometry: Clues for MS pathogenesis. *PLoS One*, *9*(9), e107649. https://doi.org/10.1371/journal.pone.0107649

Robinson, A. P., Zhang, J. Z., Titus, H. E., Karl, M., Merzliakov, M., Dorfman, A. R., Karlik, S., Stewart, M. G., Watt, R. K., Facer, B. D., Facer, J. D., Christian, N. D., Ho, K. S., Hotchkin, M. T., Mortenson, M. G., Miller, R. H., & Miller, S. D. (2020). Nanocatalytic activity of clean-surfaced, faceted nanocrystalline gold enhances remyelination in animal models of multiple sclerosis. *Scientific Reports*, *10*(1), 1936. https://doi.org/10.1038/s41598-020-58709-w

Rodgers, J. M., Robinson, A. P., & Miller, S. D. (2013). Strategies for protecting oligodendrocytes and enhancing remyelination in multiple sclerosis. *Discovery Medicine*, *16*(86), 53–63.

Rone, M. B., Cui, Q. L., Fang, J., Wang, L. C., Zhang, J., Khan, D., Bedard, M., Almazan, G., Ludwin, S. K., Jones, R., Kennedy, T. E., & Antel, J. P. (2016). Oligodendrogliopathy in multiple sclerosis: Low glycolytic metabolic rate promotes oligodendrocyte survival. *The Journal of Neuroscience*, *36*(17), 4698–4707. https://doi.org/10.1523/JNEUROSCI.4077-15.2016

Rosko, L., Smith, V. N., Yamazaki, R., & Huang, J. K. (2019). Oligodendrocyte bioenergetics in health and disease. *The Neuroscientist*, *25*(4), 334–343. https://doi.org/10.1177/1073858418793077

Sim, F. J., Zhao, C., Penderis, J., & Franklin, R. J. (2002). The age-related decrease in CNS remyelination efficiency is attributable to an impairment of both oligodendrocyte progenitor recruitment and differentiation. *The Journal of Neuroscience*, *22*(7), 2451–2459. https://doi.org/10.1523/JNEUROSCI.22-07-02451.2002

Simons, M., & Nave, K. A. (2015). Oligodendrocytes: Myelination and axonal support. *Cold Spring Harbor Perspectives in Biology*, *8*(1), a020479. https://doi.org/10.1101/cshperspect.a020479

Smarr, C. B., Yap, W. T., Neef, T. P., Pearson, R. M., Hunter, Z. N., Ifergan, I., Getts, D. R., Bryce, P. J., Shea, L. D., & Miller, S. D. (2016). Biodegradable antigen-associated PLG nanoparticles tolerize Th2-mediated allergic airway inflammation pre- and postsensitization. *Proceedings of the National Academy of Sciences of the United States of America*, *113*(18), 5059–5064. https://doi.org/10.1073/pnas.1505782113

Terry, R. L., Ifergan, I., & Miller, S. D. (2016). Experimental autoimmune encephalomyelitis in mice. *Methods in Molecular Biology*, *1304*, 145–160. https://doi.org/10.1007/7651_2014_88

Tintore, M., Vidal-Jordana, A., & Sastre-Garriga, J. (2019). Treatment of multiple sclerosis - success from bench to bedside. *Nature Reviews. Neurology*, *15*(1), 53–58. https://doi.org/10.1038/s41582-018-0082-z

Titus, H. E., Chen, Y., Podojil, J. R., Robinson, A. P., Balabanov, R., Popko, B., & Miller, S. D. (2020). Pre-clinical and clinical implications of "inside-out" vs. "outside-in" paradigms in multiple sclerosis etiopathogenesis. *Frontiers in Cellular Neuroscience*, *14*, 599717. https://doi.org/10.3389/fncel.2020.599717

Weiner, H. L. (2009). The challenge of multiple sclerosis: How do we cure a chronic heterogeneous disease? *Annals of Neurology*, *65*(3), 239–248. https://doi.org/10.1002/ana.21640

Xu, H., Dzhashiashvili, Y., Shah, A., Kunjamma, R. B., Weng, Y. L., Elbaz, B., Fei, Q., Jones, J. S., Li, Y. I., Zhuang, X., Ming, G. L., He, C., & Popko, B. (2020). M(6)a mRNA methylation is essential for oligodendrocyte maturation and CNS myelination. *Neuron*, *105*(2), 293–309. https://doi.org/10.1016/j.neuron.2019.12.013

Yanes, O., Clark, J., Wong, D. M., Patti, G. J., Sánchez-Ruiz, A., Benton, H. P., Trauger, S. A., Desponts, C., Ding, S., & Siuzdak, G. (2010). Metabolic oxidation regulates embryonic stem cell differentiation. *Nature Chemical Biology*, *6*(6), 411–417. https://doi.org/10.1038/nchembio.364

Zhou, Y., Zhou, B., Pache, L., Chang, M., Khodabakhshi, A. H., Tanaseichuk, O., Benner, C., & Chanda, S. K. (2019). Metascape provides a biologist-oriented resource for the analysis of systems-level datasets. *Nature Communications*, *10*(1), 1523. https://doi.org/10.1038/s41467-019-09234-6

SUPPORTING INFORMATION

Additional supporting information can be found online in the Supporting Information section at the end of this article.

How to cite this article: Titus, H. E., Xu, H., Robinson, A. P., Patel, P. A., Chen, Y., Fantini, D., Eaton, V., Karl, M., Garrison, E. D., Rose, I. V. L., Chiang, M. Y., Podojil, J. R., Balabanov, R., Liddelow, S. A., Miller, R. H., Popko, B., & Miller, S. D. (2022). Repurposing the cardiac glycoside digoxin to stimulate myelin regeneration in chemically-induced and immune-mediated mouse models of multiple sclerosis. *Glia*, *70*(10), 1950–1970. https://doi.org/10.1002/glia.24231